HHS Public Access

Author manuscript

Stem Cells. Author manuscript; available in PMC 2015 April 15.

Published in final edited form as:

Stem Cells. 2014 April ; 32(4): 886–901. doi:10.1002/stem.1599.

Wnt7b is an important intrinsic regulator of hair follicle stem cell homeostasis and hair follicle cycling

Eve Kandyba[1,2] and **Krzysztof Kobielak**[1,2,*]

[1]Eli and Edythe Broad CIRM Center for Regenerative Medicine and Stem Cell Research, University of Southern California, Los Angeles, CA

[2]Department of Pathology, University of Southern California, Los Angeles, CA

Abstract

The hair follicle (HF) is an exceptional mini-organ to study the mechanisms which regulate HF morphogenesis, cycling, hair follicle stem cell (hfSCs) homeostasis and progeny differentiation. During morphogenesis, Wnt signaling is well characterized in the initiation of HF patterning but less is known about which particular Wnt ligands are required and whether individual Wnt ligands act in an indispensable or redundant manner during postnatal hfSCs anagen onset and HF cycle progression. Previously, we described the function of the Bone morphogenetic protein (BMP) signaling target gene WNT7a in intrinsic regulation of hfSCs homeostasis *in vivo*. Here, we investigated the role of Wnt7b, which was also intrinsically up-regulated in hfSCs during physiological and precocious anagen after BMP inhibition *in vivo*. We demonstrated Wnt7b to be a direct target of canonical BMP signaling in hfSCs and using Wnt7b conditional gene targeting during HF morphogenesis revealed disrupted HF cycling including a shorter anagen, premature catagen onset with overall shorter hair production and diminished HF differentiation marker expression. Additionally, we observed that postnatal ablation of Wnt7b resulted in delayed HF activation, affecting both the HG and bulge hfSCs but still maintaining a two-step sequence of HF stimulation. Interestingly, Wnt7b cKO hfSCs participated in re-formation of the new HF bulge, but with slower self-renewal. These findings demonstrate the importance of intrinsic Wnt7b expression in hfSCs regulation and normal HF cycling and surprisingly reveal a non-redundant role for Wnt7b in the control of HF anagen length and catagen entry which was not compensated by other Wnt ligands.

Keywords

Hair follicle stem cells; WNT signaling; Wnt7b

[*]To whom correspondence should be addressed: The Broad CIRM Center for Regenerative Medicine and Stem Cell Research, Department of Pathology, University of Southern California, 1425 San Pablo Street, BCC-513, Los Angeles, California 90033, Tel: (323) 442-3208, Fax: (323) 442-7832, kkobiela@med.usc.edu (please use for all correspondence).

Eve Kandyba: Conception and design, Collection and/or assembly of data, Data analysis and interpretation, Manuscript writing
Krzysztof Kobielak: Conception and design, Data analysis and interpretation, Manuscript writing, Final approval of manuscript

INTRODUCTION

The hair follicle (HF) provides a highly informative model system to study the underlying mechanisms that regulate hair follicle stem cell (hfSCs) homeostasis and progeny differentiation. HF development results from a co-ordinated series of epithelial-mesenchymal signals which initiate epithelial down-growths which develop and differentiate to form mature HFs [1–3]. Mature HFs are fully established during the growth phase (anagen), after which the lower epithelial portion of HFs undergo degeneration (catagen) and rest (telogen) with following re-growth of the HFs at the next anagen cycle[4]. The upper permanent, non-cycling portion of each HF forms the hair bulge, a reservoir of hfSCs containing label-retaining, slow cycling cells (LRCs) marked by CD34 expression [5–9]. During the telogen-anagen transition, activation of the proliferative hair germ (HG), a responsive region directly between the bulge and the dermal papillae (DP), precedes bulge hfSCs activation to promote rapid initial hair growth [10]. Upon hfSCs activation, the bulge then fuels the regenerating HF, driving downward growth and formation of the actively dividing proliferative hair matrix (Mx) progenitor which terminally differentiate to generate the inner root sheath (IRS) and hair shaft (HS). Normal HF growth and cycling is maintained via a careful balance of Mx cell proliferation versus terminal differentiation arising from signaling cues which are, as yet, not fully understood.

Although multiple signaling pathways converge to govern HF development, differentiation and postnatal cycling [2, 11–15], the canonical wingless-type MMTV integration site family (Wnt) signaling in particular is believed to be a fundamental pre-requisite for HF morphogenesis and also later in HFs differentiation [2, 16]. Proper HS differentiation is dependent on Wnt signaling and alterations in this pathway result in numerous HF abnormalities [17–19]. Moreover, the Wnt reporter gene TOPGAL as well as BAT-gal is most active in the differentiating pre-cortical and cortical cells of the developing HS [20, 21]. The Wnt ligands, their antagonists (such as dikkopf 1, Dkk1) and Wnt receptors, frizzleds (Fzd) have complex spatio-temporal expression patterns within developing epidermis and HFs [2, 22–24] suggesting possible redundancy between some Wnt ligands and receptors. Indeed, studies employing *in vivo* genetic modulation of canonical Wnt signaling have offered significant insight into the function of canonical Wnt signaling during skin and HF morphogenesis reporting that elevated β-catenin stabilization induces *de novo* HF development [19, 25]. In contrast, β-catenin-deficiency precludes HF formation completely [18] and stabilization of β-catenin during postnatal telogen phase promotes precocious hfSCs activation and accelerated HF growth [26, 27]. Moreover, when Wnt signaling was inhibited by ectopic expression of Dkk1 in the skin of transgenic mice, this resulted in a complete failure of hair placode formation [24]. Although Wnt signaling is required for HFs pattern initiation, regulation of hfSCs homeostasis, HFs cycling and differentiation, much less is known about which particular Wnt ligands are required in these processes and whether individual Wnt ligands act in an indispensable or redundant manner.

Recently, we identified Wnt7b as a putative target of BMP signaling in hfSCs *in vivo* [28]. Here, we identify and characterize the defects in HF development, differentiation and hfSCs homeostasis arising from Wnt7b-deficiency by employing conditional gene targeting to specifically ablate Wnt7b during HF morphogenesis and postnatally in adult hfSCs. We

revealed a spatio-temporal expression pattern of endogenous Wnt7b protein during HF development and demonstrate that deletion of Wnt7b (Wnt7b cKO) during HF morphogenesis resulted in disrupted HF cycling including a shorter growth phase, premature catagen onset and shorter hair coat production with diminished HF differentiation marker expression. Furthermore, postnatal ablation of Wnt7b in hfSCs resulted in significantly delayed HF activation suggesting Wnt7b could function as a key component required for normal hfSCs activation during the physiological telogen-anagen transition, which determine normal HFs anagen length.

Thus, our results reveal unexpected findings that, contrary to the view that Wnt ligands may act with promiscuous redundancy, particular Wnt ligands may possess non-redundant functions during HF development, differentiation and postnatal hfSCs homeostasis. These data also support our previously published model comprising an additional Wnt ligand component, Wnt7b, to the pathways integral cross-talk between BMP and WNT in hfSCs regulation. Our findings lend support to our hypothesis that inhibition of BMP signaling primes the HF towards activation in a Wnt-ligand dependent manner and reveal direct binding of active phospho-Smads (pSmads) within the Wnt7b promoter region. Collectively, these results provide new insights into the functions of Wnt7b functions in HF development and hfSCs homeostasis.

MATERIALS AND METHODS

Generation, genotyping and manipulation of Wnt7b transgenic mouse lines

Keratin 14 (K14) promoter driven Cre recombinase mice and K15-CrePR transgenic mice, inducible by topical administration of RU486 were obtained from Jackson Laboratories [9, 29]. Conditional floxed alleles of Wnt7b were obtained from Jackson Laboratories [30]. Rosa26-STOP-eYFP (Yellow Fluorescent Protein) mice were obtained from Jackson Laboratories [31]. To generate mice lacking Wnt7b in the skin epithelium during morphogenesis, $Wnt7b^{fl/fl}$ mice were crossed with K14Cre mice (Wnt7b cKO) or, alternatively, with K15CrePR mice to generate offspring with inducible, targeted Wnt7b ablation (Wnt7b cKO^{RU}) in the hfSCs population following RU486 treatment postnatally. Bmpr1a cKO^{RU} mice were described previously [28]. All mice were genotyped from tail snips. YFP labeling and targeted deletion of Wnt7b in hfSCs was achieved by topical application of RU486 (25mg/ml, VWR), to shaved dorsal back skin during the first postnatal telogen from P18 to P21. Following recombination events, Wnt7b-deficient cells (and all progeny) were permanently marked by YFP expression. All animal procedures were performed with the appropriate approval of the IACUC committee.

Immunostaining procedure

Cryosections for immunostaining were briefly fixed in 4% paraformaldehyde, washed in PBS and incubated in 0.1% Triton-X100 (v/v in PBS) for 10 minutes. Sections were then blocked in 10% appropriate serum (v/v in 0.1% Triton-X100/PBS) for 30 minutes at room temperature then incubated in primary antibodies overnight at 4°C. Antibodies were diluted in blocking solution at the following dilutions: Ae13 (1:100; Santa Cruz), Ae15 (1:25; Santa Cruz), Gata3 (1:75, Santa Cruz), K1 (1:300; Gifted by C. Jamora), K5 (1:300; Gifted by C.

Jamora), Ki67 (1:300; Novocastra), Loricrin (1:300; Gifted by C. Jamora), YFP (1:3000; anti-GFP Abcam), Wnt7b (1:100, Abcam), P-cadherin (1:100; R&D), Lef-1 (1:100; Cell Signaling), β-catenin (1:300; Sigma-Aldrich). Sections were washed in PBS and incubated with secondary antibodies, diluted at 1:300 in appropriate blocking solution for 45 minutes at room temperature in the dark. Sections were washed thoroughly with PBS, counterstained with DAPI to label nuclei (DAPI counterstaining was omitted for triple CD34/P-cadherin/Ki67 staining), mounted and stored at 4°C until ready for analysis. Additional tissue processing was performed to obtain defined YFP staining (for lineage tracing experiments) where skin samples were fixed in 4% paraformaldehyde for 2 hours at 4°C and then immersed in 30% sucrose (w/v in PBS) overnight at 4°C prior to embedding in OCT for sectioning and staining as described above. Immunohistochemistry (IHC) using the VIP staining kit (purple stain, Vector Laboratories) was performed on paraffin embedded samples, sectioned at 7μm thickness. Briefly, paraffin sections were hydrated, antigen retrieval was performed by using Citrate buffer (pH 6.0) for 20 minutes in a pressure cooker, sections were washed in PBS and then blocked in 0.3% hydrogen peroxide for 10 minutes. IHC staining was then performed according to the manufacturer's instructions.

Synchronized hair follicle (HF) activation experiments

Hair was waxed from a ~1cm^2 area of dorsal back skin from Con and Wnt7b cKO mice during the prolonged postnatal telogen to induce synchronized HF activation and promote the transition from telogen to anagen. Images and biopsies were collected every 2–3 days until HF regeneration was complete (~3 weeks).

TUNEL staining

To detect cell apoptosis, we used the in situ cell death detection kit (Roche, Pleasanton, CA) according to the manufacturer's instructions.

Hair follicle analysis (number, length, type)

HF and type were examined in Con and Wnt7b cKO mice. The length and type of Con and Wnt7b cKO hairs were examined under a dissection microscope (Leica). Approximately 500 hair follicles were examined from Con and Wnt7b cKO mice (n=3) and the length of 20 hairs of each type from Con and Wnt7b cKO mice were measured.

In vivo hfSC ChIP Assay

In vivo ChIP was performed using cells directly FACS sorted from Bmpr1a gain-of-function K15-GFP+/dTg mice at P21 [28, 32] with or without Doxy food (from P18–P21) in the presence of phosphatase inhibitors. Approximately 3×10^6 K15-GFP cells (bulge hfSCs) were isolated from both control and dTg samples and fixed in 1% formaldehyde and then quenched with 0.125M glycine. Cells were then snap-frozen and stored at −80°C until required for further processing. Samples were prepared using a Qiagen EpiTect ChIP OneDay Kit according to the manufacturer's instructions. DNA was sheared by sonication to an average length of 500bp (as measured by electrophoresis) and P-Smad1/5/8 (rabbit, Cell Signaling, 1:50) or control IgG (rabbit, Sigma, 1:50) was added to each sample to form immunocomplexes. Putative Smad binding sites were identified with BioBase Promoter

analysis software and 5' upstream ChIP primer sequences were designed (with the aid of Ensemble software) based on clustering of Smad binding sites (primarily Smad1/5/8) with PCR performed using Input or immunoprecipitated DNA and primers designed to amplify a specific region of the Wnt7b promoter.

Promoter analyses for SMAD binding sites (SBE)

Computer predictions (Biobase, **BKL TRANSFAC** promoter analyses software) of SMAD 1/5/8 binding sites (SBE) within the Wnt7b promoter region.

Fluorescence-activated cell sorting (FACS) analysis of HF bulge markers

Analysis of bulge, hair follicle stem cells (hfSCs) from adult mouse dorsal back skin was performed as described previously [28]. For hfSCs CD34 marker expression analysis, telogen (P18 Con/Wnt7b cKO; P21, P45, YFP+ Con^{Dil}/Wnt7b cKO^{Dil}) HF cell suspensions were stained with the following antibodies, anti-α6-integrin conjugated to PE (1:200; BD Pharminigen) and anti-CD34 coupled to Alexafluor-700 (1:50; BD eBioscience). Cells were gated first for live cells (absence of DAPI incorporation) then for basal hfSCs: α6-$integrin^{High}$/$CD34^{High}$ labeled cell fraction (for the overall hfSCs number in the bulge). For RU486 Dilution Lineage Tracing experiments the basal fraction of bulge hfSCs were analyzed for presence YFP labeled cells. Basal hfSCs: YFP+/α6-$integrin^{High}$/$CD34^{High}$ labeled cell fractions were analyzed with a FACS Aria cell sorter (BD Biosciences equipped with FACS DiVa software).

RU486 Dilution for Lineage Tracing Experiments of YFP labeled hfSCs

One low dose of RU486 (1× 2.5mg topical application; Dilution, ^{Dil}) was administered to the shaved dorsal backskin of P18 Con^{Dil} and Wnt7b cKO^{Dil} mice to label approximately one or two cells per telogen HF in both Con^{Dil} and Wnt7b cKO^{Dil} HFs. At P21 (in the first postnatal telogen) and P45, (following the end of the first postnatal HF cycle when both Con^{Dil} and Wnt7b cKO^{Dil} HFs were morphologically observed in the second, prolonged postnatal telogen) hfSCs were isolated and prepared for FACs analysis as described above.

Quantification of YFP+ cells in Con^{Dil} and Wnt7b cKO^{Dil} telogen HFs

For quantification of the YFP+ labeled cells of Con^{Dil} and Wnt7b cKO^{Dil} HFs in the first and second postnatal telogen (P21 and P45), the number of double YFP+/DAPI cells were counted per HF and representative images provided in the Results section (P21, n=15; P45, n=9).

RESULTS

Generation of mice lacking Wnt7b in the epidermis and hair follicles

In situ hybridization studies have suggested that numerous Wnt ligands are expressed within developing skin and hair, including Wnt7b [24]. However, the cutaneous expression profile of endogenous Wnt7b protein as well as its function has not yet been determined during hair development and postnatal cycling. Therefore, first we performed immunohistochemistry (IHC) directed against Wnt7b on sections of wild type (Con) mouse back skin to determine

the endogenous expression pattern of Wnt7b during early hair follicle (HF) morphogenesis between embryonic (E) day E14.5 and E18.5 (Fig. 1C–E). At E14.5, strong cytoplasmic Wnt7b expression was localized to the simple basal skin epithelium (Fig. 1C). At E16.5, Wnt7b expression was localized throughout all developing epidermal layers and in emerging hair germs (Fig. 1D) and by E18.5, Wnt7b was expressed in the epidermis and in developing HFs (Fig. 1E). Wnt7b expression was largely excluded from the underlying dermal tissue with only subcutaneous muscle tissue staining positive (Fig. 1C, D', asterisk). Early developmental lethality of Wnt7b knockout mice at E9.5 due to improper placental development, [33] has impeded the study of Wnt7b function in skin and HF development. Therefore, to overcome this obstacle, we used a Cre-LoxP approach to inactivate Wnt7b in the developing epithelium in a tissue-specific manner using conditional floxed alleles (Fig. 1A) [30]. To this end, we generated transgenic mice that were conditionally deficient for epithelial Wnt7b (Wnt7b cKO) using a well characterized keratin-14 (K14) promoter driven Cre recombinase (Fig. 1A) [29]. The K14 promoter activity begins in developing epithelia from approximately E10 and then continues to drives Cre expression in adult epidermis and HFs [34]. To visualize and compare potential phenotypic changes arising from targeted Wnt7b deletion, control and mutant Wnt7b cKO mice were also crossed upon the ROS26-STOP-eYFP reporter background as an indicator of genetic recombination and to permanently YFP-label K14-derived tissue and progeny (Fig. 1A) [31]. PCR genotyping was used to verify mouse genotypes using primers specific for the floxed and wild type alleles of Wnt7b in combination with YFP+ reporter expression (Fig. 1B). Wnt7b immunohistochemistry was performed to verify efficient genetic recombination and ablation of Wnt7b in Wnt7b cKO skin at E14.5, E16.5 and E18.5 (Fig. 1C', D', E' respectively), using Con back skin as a positive experimental control (Fig. 1C, D, E, respectively).

Normal primary and secondary hair placode initiation following Wnt7b deletion

As Wnt7b protein was expressed during early hair development (Fig. 1C–E) we next examined whether loss of Wnt7b during embryogenesis affected initial hair placode formation. We employed our K14-driven YFP+ reporter expression system to visualize YFP + HF placode formation at different stages of HF development (between E14.5–18.5), identifying hair placodes as bright YFP+ aggregates within the developing epithelium. Primary hair placode formation begins at approximately E14.5 with secondary hair placode initiation beginning slightly later around E16. At E14.5, E16.5 and E18.5 we observed similar level of epidermal YFP+ expression in both Con and Wnt7b cKO embryos (Fig. S1A', 1C', 1D'), however, at E15.5, Wnt7b cKO embryos displayed temporally reduced YFP expression (Fig. S1B'). Furthermore, we observed comparable initiation of YFP+ placode formation between Con and Wnt7b cKO in primary and secondary hair morphogenesis waves (Fig. S1E–H') suggesting Wnt7b expression may not be required for initiation of hair placode formation. Quantification of HF numbers (Fig. S1I, n=7) at late stage gestation (E18.5) and postnatally at P2 revealed comparable numbers of HFs in both Con and Wnt7b cKO littermates, suggesting Wnt7b-deficiency did not perturb proper HF number during morphogenesis. However, at all developmental stages (and throughout adulthood) YFP+ Wnt7b cKO mutant mice were consistently smaller than YFP+ Con littermates (Fig. S1A–D'; Fig. S1J–J').

Proper epidermal differentiation following K14-driven Wnt7b ablation

As endogenous Wnt7b protein expression was detected in developing skin epidermis (Fig. 1C–E), we next examined whether loss of Wnt7b affected normal epidermal terminal differentiation and barrier formation using immunofluorescence directed against known epidermal differentiation markers, Keratin1 (K1) and Loricrin in YFP+ Con and Wnt7b cKO back skin at E18.5 (Fig. S2A–B'). Both YFP+ Con and Wnt7b cKO epidermis displayed comparable YFP+ expression (green) and cytoplasmic K1 (red channel) expression was strongly localized to the suprabasal epidermal layers (Fig. S2A–A'). Moreover, YFP+ Con and Wnt7b cKO epidermis both stained for loricrin (red channel) expression in the upper differentiating layers of epidermis (Fig. S2B–B') and at birth both Con and Wnt7b cKO pups demonstrated proper epidermal barrier function by dye exclusion assay (data not shown). Together, these data indicate Wnt7b-deficiency does not perturb proper epidermal differentiation and epidermal barrier formation.

Loss of Wnt7b results in perturbed hair follicle development and differentiation with aberrant hair shaft production

To investigate the consequences of Wnt7b ablation during HF development, we examined the overall appearance of the hair coat in Con and Wnt7b cKO mice from P5 to P18 (Fig. 1F–J') during hair morphogenesis. At P5, Wnt7b cKO mutants were considerably smaller in size than Con littermates and displayed lighter skin pigmentation (Fig. 1F). By P10, Wnt7b cKO mutant mice remained smaller in size than Con littermates and were significantly thinner with diminished dorsal (Fig. 1G) and ventral (data not shown) hair coat production. At P18, Wnt7b cKO mice presented visible but sparse hair in comparison to Con littermates (Fig. 1H). Close examination of YFP+ Con (Fig. 1I, I') and Wnt7b cKO (Fig. 1J, J') dorsal skin at P7 clearly showed Wnt7b cKO skin to be less pigmented (Fig. 1J) with fewer visible hair shafts (HS) on the skin surface (Fig. 1J') compared to Con littermates (Fig. 1I, I'). Moreover, HS production in Wnt7b cKO mice appeared less uniform and thinner in appearance (Fig. 1J, J') suggesting perturbed HF development and defective HS differentiation. In contrast, Con skin was highly pigmented (Fig. 1I, I') with robust, evenly spaced visible HS protruding from the skin surface, lying flat along the YFP+ dorsal epithelium (Fig. 1I'). We observed that Wnt7b cKO mice were viable, fertile and able to survive for over one year, but remained comparatively smaller than Con mice throughout adulthood (Fig. S1J–J').

To further examine the implications of Wnt7b-deficiency upon proper HF differentiation, we performed immunofluorescence directed against a panel of known HF differentiation markers in Con and Wnt7b cKO anagen HFs. We observed strong ae13 expression, a marker of the hair cortex, in the cortical layers of Con HFs (Fig. 1K, arrow) whereas expression was weaker in Wnt7b cKO cortical layers (Fig. 1K', arrow). Proper expression of ae15, a marker of the inner root sheath (IRS) layer and medulla, was observed in Con anagen HFs (Fig. 1L, arrows), however, ae15 expression was greatly diminished in Wnt7b cKO anagen HFs (Fig. 1L'). Distinct nuclear GATA3 staining, a known transcription factor essential for IRS differentiation, was observed in the differentiating IRS layers of Con HFs (Fig. 1M), however, nuclear GATA3 was weaker in the IRS of Wnt7b cKO anagen HFs (Fig. 1M').

Collectively, these data suggest that Wnt7b may play an important role for proper HF differentiation.

Perturbed hair follicle cycling and shorter pelage coat production after Wnt7b inhibition

The perturbed hair coat production in Wnt7b cKO mutant mice (Fig. 1F–J') suggested disrupted HF development. Therefore, to investigate whether loss of Wnt7b affected the normal HF cycle, we analyzed back skin from Con and Wnt7b cKO mice from P2–P45 (Fig. 2A). Con mice displayed normal hair cycle progression (Fig. 2A, top panel) and were used as a comparison for Wnt7b cKO mutant mice (Fig. 2A, lower panel). We observed considerable hair cycle disruption in Wnt7b cKO mutant HFs. At P2, Wnt7b cKO anagen HFs were smaller and less developed than anagen Con HFs, by P5, we observed slower Wnt7b cKO HFs anagen down growth into the underlying dermis and adipose tissue and Wnt7b cKO hair barely reached half of the full length of Con anagen hair and half of regular skin deepness observed in Con anagen HFs at the same time point (Fig. 2A, P2 and P5, respectively). Surprisingly, by P10, Wnt7b cKO HFs had already begun to regress indicating premature catagen onset (Fig. 2A, P10). Interestingly, Wnt7b cKO primary guard HFs appeared less affected than secondary HFs. By P18, both Con and Wnt7b cKO HFs had progressed to telogen (Fig. 2A, P18) but, unlike Con HFs which were activated at P21, telogen-anagen progression was not initiated in Wnt7b cKO HFs until approximately P24 (Fig. 2A, P24 lower panel) however both Con and Wnt7b cKO HFs progressed to telogen by P45 (Fig. 2A). During the first postnatal anagen hair cycle progression, Wnt7b cKO HFs were consistently smaller and thinner than Con HFs and failed to extend deeply into the dermis during the hair cycle (Fig. 2A, P30 lower panel). Collectively, these data demonstrate that Wnt7b may be required to maintain the proper length of the anagen phase as its absence resulted in precocious catagen with HF degeneration (Fig. 2B).

Next, to investigate whether the disruption to the HF cycle caused by Wnt7b-deficiency resulted in aberrant hair type and/or length, we analyzed plucked telogen HFs from Con and Wnt7b cKO mice at P19 after HF morphogenesis was completed. Analysis of control and Wnt7b cKO depilated hair revealed all four hair types were present (guard, awl/auchene, zigzag) at comparable ratios (Fig. 2C). However, Wnt7b cKO HFs appeared less pigmented than Con HFs (Fig. 2D) and each of the hair types of Wnt7b cKO mice were considerably shorter in length (approximately 40% shorter) than Con littermate hairs (Fig. 2E, F). Collectively, these results suggest Wnt7b may have a potential role in hair cycle length determination, proper HF differentiation and potentially function as a key component of HF activation during the telogen to anagen transition.

Wnt7b is expressed during hair follicle postnatal cycling

As we demonstrated, endogenous Wnt7b protein was abundantly expressed in epidermis and HFs during embryonic development (Fig. 1C–E). Since we observed perturbed HFs cycling, we would like to further determine the pattern of Wnt7b expression in postnatal hair cycling. Thus, we performed IHC against Wnt7b on sections of wild type (Con) mouse back skin between P5–P30 (Fig. 2G–K). At P5, Wnt7b expression was observed in the outer root sheath (ORS) of HFs (Fig. 2G), extending downwards from the sebaceous gland to (Fig. 2G'), and including, the developing hair Mx progenitors and hair shaft (HS) (Fig. 2G). At

P18, during the first postnatal telogen, Wnt7b expression was barely visible in the hair germ (HG; Fig. 2H and inset) and, at P21, during the telogen to anagen transition (when HG cells and bulge - hair follicle stem cells (hfSCs) become activated to drive the next hair cycle) Wnt7b expression was strongly expressed in the activated HG and lower bulge hfSCs (Fig. 2I and inset). At P24, during early anagen, cytoplasmic Wnt7b expression was localized to ORS cells of re-growing, anagen HFs and in the proliferative hair Mx progenitors in the HF bulb (Fig. 2J, J'). By P30, during mid anagen, Wnt7b was expressed throughout the differentiating layers of adult HFs (Fig. 2K). These Wnt7b expression data correlate well with the phenotype we observed in Wnt7b cKO and further suggest a potential role for Wnt7b during HF development, differentiation and postnatal cycling.

Precocious degeneration of HFs with early catagen onset and a prolonged telogen after Wnt7b inactivation

Cyclic phases of HF growth and degeneration are well characterized during the mouse HF cycle. We observed perturbed hair cycle progression in Wnt7b cKO HFs (Fig. 2A–B) and shorter hair coat production (Fig. 2E–F). Therefore, to further dissect the role of Wnt7b during the hair cycle, we performed Ki67 immunofluorescence to detect cell proliferation (Fig. 3A–F') and degeneration by TUNEL staining to demonstrate cell apoptosis (Fig. 3G–K'). During the anagen phase of the hair cycle, the Mx progenitor cells actively proliferate to generate progeny which progressively differentiate to form all layers of the HS and IRS. At P5 and P8 we observed that anagen Wnt7b cKO HFs were consistently smaller and thinner (Fig. 3A', B') than Con HFs (Fig. 3A, B) during the hair cycle, however, the Mx of Wnt7b cKO HFs still showed abundant nuclear Ki67 expression. Significantly, at P10, Wnt7b cKO HFs did not express any Ki67 marker and were morphologically degenerating (Fig. 3C') whereas Con HFs still displayed strong nuclear Ki67 staining at Mx bulb of anagen HFs (Fig. 3C). By P14, Wnt7b cKO HFs had progressed to telogen and did not express Ki67 (Fig. 3D'), in contrast, Con HFs remained in anagen and still displayed cell proliferation in the lower hair bulb Mx progenitor cell population (Fig. 3D). During the physiological telogen-anagen transition at P21, Con HFs (Fig. 3E) displayed strong nuclear Ki67 staining in the HG and lower bulge hfSCs, however, Wnt7b cKO HFs failed to transition towards anagen and remained quiescent in telogen lacking Ki67 staining (Fig. 3E'). At P24, Con HFs had progressed into early anagen and displayed abundant Ki67 expression in the developing Mx (Fig. 3F), whereas, Wnt7b cKO HFs were just activated and with strong nuclear Ki67 staining observed in the activated HG (Fig. 3F'). These data indicate faster withdrawal of cell proliferation in Wnt7b cKO HFs and premature catagen onset.

To examine whether the precocious withdrawal of cell proliferation observed in Wnt7b cKO HFs was accompanied by earlier HF apoptotic events during premature catagen, we performed TUNEL staining (Fig. 3G–K'). We confirmed that the onset of catagen began around P14 in Con HFs when one or two TUNEL positive cells were detected in the Mx progenitor cells in the lower hair bulb (Fig. 3J), however, at the same time point Wnt7b cKO HFs were already in telogen and TUNEL negative (Fig. 3J'). Surprisingly, the first TUNEL positive cells in Wnt7b cKO HFs were observed much earlier at P8 in the hair bulb Mx progenitor cells (Fig. 3H') indicating premature catagen onset (precocious HF involution),

with anagen Con HFs still TUNEL negative (Fig. 3H). Indeed, strong nuclear TUNEL staining could be observed in the regressing epithelial strand by P10 in Wnt7b cKO HFs (Fig. 3I', arrow), in contrast to TUNEL negative proliferating anagen Con HFs at the same point (Fig. 3I). At P5 and P18 both Con and Wnt7b cKO HFs were TUNEL negative either in proliferating anagen (Fig. 3G, G') or quiescent telogen (Fig. 3K, K').

As Wnt signaling is believed to promote cell proliferation events, we next examined whether loss of Wnt7b disrupted proper Wnt signaling in the matrix progenitor cell population and performed immunohistochemistry directed towards Lef-1, a downstream effector of Wnt signaling, during hair morphogenesis from P2–P8 (Fig. S3A–C; Fig. 3L–M). We observed that both Con (Fig. S3A–C) and Wnt7b cKO (Fig. S3A'–C') HFs displayed nuclear Lef-1 expression in the Mx progenitor cells within the hair bulb. However, at higher magnification, we observed a reduced number of Lef-1 positive cells (with less intense nuclear Lef-1 staining) in Wnt7b cKO Mx cells (Fig. 3L') when compared with Con HFs (Fig. 3L) at P5. Furthermore, quantification of the number of Lef-1 positive Mx cells in Con and Wnt7b cKO HFs (Fig. 3M) confirmed considerably less Lef-1 positive Mx cells in the hair bulge of Wnt7b cKO HFs. Analysis of β-catenin IHC during HF development from P2–P8 revealed a comparable level of staining of nuclear β-catenin in both Con and Wnt7b cKO skin (Fig. 3N–N' and Fig. S3D–F'), although we detected less β-catenin positive cells in Mx of Wnt7b cKO HFs, but this could reflect the overall smaller size of Wnt7b cKO HFs when compared to Con. Collectively, these findings demonstrate that upon Wnt7b ablation during HF development, the HF cycle is severely disrupted and support a potential role for Wnt7b in HF cycle length determination and cell proliferative events.

A non-redundant function of Wnt7b to promote bulge hfSCs and HG activation

We observed delayed telogen-anagen (T-A) transition in Wnt7b cKO HFs (Fig. 2A–B; Fig. 3E–F') suggesting defective HF activation following Wnt7b ablation. Therefore, to examine whether loss of Wnt7b differentially affected activation of the bulge hfSCs population or the secondary hair germ (HG) we performed triple IF targeting CD34 (a hfSC marker, red), P-cadherin (high expression in the hair germ, see Greco et al., 2009, green) and Ki67 (to indicate proliferating cells, blue) at P21 (Fig. 4A–B) and P24 (Fig. 4C–D). At P21, we observed nuclear Ki67 staining primarily in the HG region of Con HFs with minimal cell proliferation in the bulge hfSCs (Fig. 4A and inset, arrows). In contrast, nuclear Ki67 staining was undetectable in P21 Wnt7b cKO HFs in either the bulge hfSCs or HG region (Fig. 4B and inset). However, during Wnt7b cKO HF T-A transition at P24, nuclear Ki67 staining was observed primarily in the HG region indicating HF activation (Fig. 4D and inset, arrows). By P24, Con HFs had already progressed into anagen (following initial rapid proliferation of the HG to form the regenerating hair structure below the CD34 positive bulge) and strong membranous P-cadherin expression localized with nuclear Ki67 positive cells in the developing ORS and Mx of regenerating Con HFs (Fig. 4C). Quantification of these stainings revealed that during postnatal T-A transition in Con HFs at P21, cell activation was observed primarily in the HG and then later in the bulge (Fig. 4E, P21 and P24, n=10 HFs counted in both time points, respectively). Thus, although Wnt7b cKO HF activation was delayed, a very similar sequence of cell activation (primarily in HG and later in bulge) was observed in Wnt7b cKO HFs at P24 (Fig. 4E, P24). These data suggest that

Wnt7b-deficiency does not perturb the sequential mechanism of HF activation and, similar to Con HFs, Wnt7b cKO HFs activate using a “two-step” mechanism [10] whereby the more responsive HG activates first to enable rapid HF activation and downgrowth with subsequent bulge hfSCs activation to fuel HF regeneration.

Furthermore, to determine whether Wnt7b ablation during morphogenesis affected the initial number of hfSCs established in the bulge in the first postnatal telogen HF, we performed FACS analysis at P18 (when both Con and Wnt7b cKO HFs were morphologically in telogen). FACS analysis using α6-integrin in conjunction with CD34 staining to label hfSCs demonstrated comparable total numbers of telogen bulge hfSCs in both Con (Fig. 4F, 39.8%) and Wnt7b cKO (Fig. 4F’, 40.0%) HFs indicating Wnt7b ablation did not affect bulge hfSCs formation. Collectively, these findings suggest that the delayed HF activation in Wnt7b cKO HFs is due to non-redundant functions of Wnt7b acting in both the bulge hfSCs and HG without affecting the initial stem cells number during the first bulge formation in the first postnatal telogen.

Delayed anagen entry in Wnt7b-deficient hair follicles following synchronized hfSC activation with overall restricted HFs down growth

To further investigate the hair phenotype generated from ablation of Wnt7b, back skin from both Con and Wnt7b cKO mice was waxed to remove any existing club hair shafts formed during hair morphogenesis and synchronize hfSCs activation. After 3 days post-waxing (dpw), we observed morphological HF activation in Con HFs which displayed transition to anagen phase with observed down-growth into the dermis (Fig. 5A), however, Wnt7b cKO HFs showed very early indications of anagen entry (Fig. 5A’). At 7dpw, mid anagen Con HFs extended deep into the dermis and visible hair shafts (Fig. 5B) could be seen, in contrast, anagen was considerably delayed in Wnt7b cKO HFs which were smaller and did not descend as deeply into the dermis compared with Con HFs (Fig. 5B’). Three days later, at 10dpw, full anagen Con HFs had produced thick, visible hair shafts which penetrated the overlying epidermis (Fig. 5C). However, Wnt7b cKO HFs at the same time point appeared thinner and did not descend as deeply into the dermis as Con follicles (Fig. 5C’). At 14dpw, Con HFs remained in anagen (Fig. 5D), at a similar depth as observed at 10dpw, similarly, Wnt7b cKO HFs follicles appeared at the same depth in the dermis as observed at 7dpw (Fig. 5D’). At 18dpw, Wnt7b cKO HFs were already in telogen (Fig. 4E’) indicating a considerably shorter HF cycle compared with Con HFs (Fig. 5E). We observed HS production in both Con and Wnt7b-deficient skin, however, Wnt7b cKO HFs displayed reduced skin pigmentation as indicated by melanocyte activation and melanin transfer to keratinocytes in anagen HFs in the depilated area (Fig. S4A–E’) suggested limited development. In addition, the HS produced by Wnt7b cKO HFs were significantly thinner than control hair (Fig. S4A–E’). At 10dpw, control skin biopsies displayed thick, strongly pigmented hair protruding from the dorsal epidermis (Fig. S4F–H’), however, Wnt7b cKO biopsied skin displayed thinner, more delicate dorsal hair (Fig. S4F–H’). When we examined the ventral side of the biopsies at 14dpw we observed thicker, anagen hair bulbs in control skin (Fig. S4I) when compared with Wnt7b KO skin (Fig. S4I’).

To examine the proliferative status of Wnt7b cKO HFs following synchronized HF activation, we performed Ki67 immunofluorescence to label actively proliferating cells within the regenerating follicles. At 3dpw, control follicles exhibited abundant nuclear Ki67 staining in the developing hair bulb region (Fig. 5F), whereas, delayed Wnt7b cKO follicles displayed less nuclear staining in the enlarged HG region (Fig. 5F'). By 7dpw, both Con (Fig. 5G) and Wnt7b cKO follicles (Fig. 5G') displayed nuclear Ki67 staining in cells of the developing ORS and in the hair Mx cells within the hair bulb region. Although Ki67 staining was also observed at 14dpw in Con (Fig. 5H) and Wnt7b cKO HFs (Fig. 5H'), Wnt7b cKO HFs already demonstrated some morphological signs of catagen. These data indicate that loss of Wnt7b significantly perturbs hfSCs homeostasis and demonstrate Wnt7b could be an important feature of hfSCs activation and that redundancy from other Wnt ligands cannot compensate fully for Wnt7b loss.

Postnatal targeted Wnt7b ablation in the bulge results in delayed hfSCs activation and telogen-anagen transition

We have previously demonstrated that Wnt7b is upregulated upon inhibition of BMP signaling in the hfSCs population *in vivo* [28] and confirmed its protein expression during the physiological telogen to anagen transition at P21 (Fig. 2I). To demonstrate whether Wnt7b is a potential target of BMP signaling in hfSCs *in vivo*, we performed Wnt7b immunohistochemistry on sections of HFs from Con^{RU} and Bmpr1a cKO^{RU} HFs where BMP signaling was specifically inhibited in the hfSCs population [28]. After targeted BMP inhibition, specifically in the HF bulge area, we observed up-regulation of Wnt7b protein expression in the activated HG and hfSCs population in Bmpr1a cKO^{RU} HFs (Fig. 6A'), in contrast to Con^{RU} HFs which did not display Wnt7b staining (Fig. 6A). These data suggest Wnt7b may have an important role in hfSCs activation and support our model whereby BMP inhibition results in the up-regulation of Wnt7b expression [28]. To validate whether Wnt7b was a direct target of BMP signaling in hfSCs *in vivo*, we used *in vivo* hfSCs ChIP assay to examine direct binding of pSmad1/5/8 to the promoter region of Wnt7b and demonstrated Wnt7b as a direct target of canonical BMP signaling in hfSCs (Fig, 6B).

To address whether loss of Wnt7b specifically in the hfSCs population could disrupt stem cells homeostasis in the hair, we generated a targeted, hfSCs specific Wnt7b loss-of-function transgenic mouse (Fig. 6C). Using this approach, along with specific inactivation of Wnt7b in hfSCs, we simultaneously labeled K15+ hfSCs by crossing these mice with a Cre-dependent YFP reporter knocked into the ubiquitously expressed Rosa26 locus (R26eYFP). Offspring from matings of K15CrePR /$Wnt7b^{fl/fl}$ / YFP mice yielded litters of the expected numbers, genotype and Mendelian ratios. RU486 (RU) was applied topically to back skin of adult mice to induce Cre-dependent recombination when HFs were in the first short, synchronized postnatal telogen at P18 and were indistinguishable at the end of the RU treatment at P21. Prior to RU treatment, $Wnt7b^{fl/fl}$ / K15CrePR / YFP (Wnt7b cKO^{RU}) mice were indistinguishable from control (Con^{RU}) animals. Three days of RU treatment (P18–P21, inset) activated YFP expression specifically in both Wnt7b cKO^{RU} and Con^{RU} HF bulges, indicating high efficiency of recombination *in vivo*, which at P21 displayed telogen, quiescent morphology. Con^{RU} (Fig. 6D) and Wnt7b cKO^{RU} (Fig. 6D') YFP+ HFs remained still in telogen at P25, due to RU treatment as previously reported [35]. However, at P28

Con^{RU} YFP labeled HFs displayed early telogen-anagen transition with activated and enlarged HG (Fig. 6E), in contrast, Wnt7b cKO^{RU} YFP+ HFs remained in telogen (Fig. 6E'). Wnt7b cKO^{RU} YFP+ HFs displayed morphological signs of anagen activation with enlarged HG (Fig. 6F'), four days after Con^{RU} YFP+ HFs, at P32. At the same time point, Con^{RU} YFP+ HFs were already in mid anagen, with HFs extending deep into the dermis, with efficient YFP labeling of the majority of the HF (Fig. 6F). By P36, YFP+ Wnt7b cKO^{RU} HFs (Fig. 6G') were in anagen with the HF extending into underlying dermis, however, the YFP+ HFs appeared thinner/smaller than Con^{RU} (Fig. 6G). Notably, at P36, Wnt7b cKO^{RU} YFP+ HFs were still at an earlier stage of anagen than Con^{RU} YFP+ HFs at P32 indicating a significant delay and restricted HF cycle progression in Wnt7b cKO^{RU} HFs.

As delayed Wnt7b cKO^{RU} YFP+ hfSCs activation was observed following Wnt7b deletion in the bulge (Fig. 6D–G'), we next performed Ki67 immunofluorescence to examine potential changes in hfSCs proliferative events following hfSCs-specific Wnt7b ablation. At P28, the YFP+ Con^{RU} HG and lower YFP+ bulge displayed strong nuclear Ki67 staining indicating early HF activation (Fig. 6H), however, at the same time point, Ki67 staining was absent in YFP+ Wnt7b cKO^{RU} HFs (Fig. 6H'). By P32, nuclear Ki67 expression was detected in the YFP+ Wnt7b cKO^{RU} HG and the YFP+ bulge hfSCs lacked Ki67 staining (Fig. 6I') whereas Con^{RU} YFP+ HFs displayed abundant nuclear Ki67 expression in the hair Mx progenitor cells (Fig. 6I). Collectively, these findings demonstrate for the first time that Wnt7b is an important component needed for hfSCs activation during the telogen-anagen transition to prime hfSCs towards activation.

Wnt7b-deficient hfSCs are capable of reforming the new HF bulge

As a consequence of the observed delay in Wnt7b-deficient hfSCs activation during T-A transition, we speculated whether there could be negative selection of Wnt7b cKO^{RU} hfSCs over time with consequently, progressive enrichment of Con hfSCs which would then proceed to reform the new bulge hfSCs population during the hair cycle. To test this hypothesis, we devised a "dilution" labeling approach, whereby we administered one low dose of RU486 (2.5mg at P18, Dilution, ^{Dil}) to Con^{Dil} and Wnt7b cKO^{Dil} mice which was sufficient to YFP+ label only one or two cells per telogen HF at P21 (Fig. 6J–J"). By marking only a few cells per telogen HF, we could then examine the enrichment of YFP+ labeled cells in the next postnatal telogen phase to determine whether Wnt7b cKO^{Dil} hfSCs could repopulate the "new" HF bulge as efficiently as Con^{Dil} hfSCs. To ensure that our dilution approach labeled comparable numbers of YFP+ Con^{Dil} and Wnt7b cKO^{Dil} cells, we performed FACS analysis of both Con^{Dil} and Wnt7b cKO^{Dil} at P21 (three days after the initial RU treatment) to examine total numbers of labeled YFP+ basal hfSCs (b-hfSCs) in the "old" bulge. Our FACS analysis revealed very similar efficiencies of YFP+ cell labeling, approximately 4% total hfSCs were labeled with YFP+ in both Con^{Dil} and Wnt7b cKO^{Dil} bulge (Figure. 6K, L vs. K', L', respectively). We hypothesized that any potential difference in YFP+ cell numbers (YFP+ b-hfSCs) observed in the next telogen cycle could be attributed to hfSCs Wnt7b-deficiency. At P45, both Con^{Dil} and Wnt7b cKO^{Dil} HFs had transitioned to the next resting telogen phase, where an "old" bulge (initially labeled) existed with a "new" bulge formed during the last hair cycle. At P45, we observed fewer YFP+

Wnt7b cKO^{Dil} b-hfSCs compared with Con^{Dil} HFs (Figure. 6M–M'') and, using FACS analysis, confirmed that YFP+ Wnt7b cKO^{Dil} b-hfSCs represented approximately 15% of the total bulge (CD34/α6-integrin positive cells), whereas, twice as many Con^{Dil} YFP+ b-hfSCs were present (30%, total YFP+ CD34/α6 positive bulge cells; Figure. 6N', O' vs. N, O). In both cases, however, we observed enrichment of P45 YFP+ hfSCs when compared to the initial P21 telogen YFP+ hfSCs, with 7.5 folds increase of number of stem cells in Con^{Dil} HFs (from ~4% at P21 to ~30% at P45, Fig.6L and 6O), and around half less, but still 3.75 fold more YFP+ stem cells enrichment in Wnt7b cKO^{Dil} (from ~4% to ~15%, Fig. 6L' and 6O'). Together, these data demonstrate that, although less effective than Con^{Dil}, Wnt7b cKO^{Dil} stem cells can support considerable enrichment of hfSCs in the next telogen HF stage and participate and establish the "new" bulge at the end of the next HF cycle. Our data suggests Wnt7b cKO hfSCs possess all the necessary qualities required for proper HF regeneration but proceed in a comparatively "slower" manner. Additionally, following a full dosage of RU486 (sixteen days from P43–P59, Fig.S5A), at 1yr of age, we observed that Wnt7b cKO^{RU} mice presented HFs which displayed efficient YFP+ labeling in both "old" and "new" bulge regions indicating that even over long periods of time, YFP+ Wnt7b cKO^{RU} could persist in high numbers and retain the ability to re-build and regenerate new hair (Fig.S5B).

DISCUSSION

Here, using genetic approaches we were able to reveal the role of Wnt7b during hair morphogenesis, HFs cycling and postnatal hfSCs homeostasis.

Wnt7b is critical for effective progression of HF down growth during anagen, but not for initiation of placode patterning during HF morphogenesis

It has been demonstrated that canonical Wnt signaling is responsible to regulate HF morphogenesis, promote hair growth and the HF cycle [24, 36–39]. Indeed, the knockout of either β-catenin or its nuclear co-transcription partners Lef1 as well as both Tcf3 and Tcf4 results in inhibition of HF morphogenesis [18, 40–42]. In contrast, excessive activation of canonical Wnt signaling leads to *de novo* hair formation during morphogenesis, accelerated hfSCs activation promoting anagen hair growth and prolonged over-expression cause tumor induction [19, 26, 27, 43]. Previous data have demonstrated abundant Wnt ligands and Fzd receptors expression at the mRNA level with overlapping spatial-temporal patterning in developing epidermis and HFs, suggesting possible redundant functions between some of the Wnt/Fzd family members *in vivo* [22, 23]. Regarding Wnt7b, previous studies have determined its RNA expression during early placode initiation in epidermis both by RT-PCR and *in situ* hybridization (ISH) and Wnt7b was also co-expressed with other Wnt ligands including Wnts 3, 4, 6, 7a, 10a, 10b and 16 in epidermal cells throughout morphogenesis [23]. Here, our findings demonstrate an expression pattern of endogenous Wnt7b protein which correlates well with the previously reported mRNA expression pattern in early epidermal development (Fig 1 C, D, E). Moreover, we demonstrated the Wnt7b protein expression pattern during hair formation and postnatal HF cycling. We revealed that loss of Wnt7b function resulted in normal hair placode initiation, proper epidermal differentiation and skin barrier formation (Fig. S1, S2), which could imply a redundant role of Wnt7b in these

processes. Although our data and previous studies have suggested possible redundancy between some Wnt ligands expressed in similar spatial-temporal patterns, surprisingly, we observed delayed HF activation with restricted overall HF down growth following loss of Wnt7b, which suggested a possible non-redundant function for Wnt7b in later stages of HF growth during morphogenesis. Such a non-redundant function for Wnt7b challenges the postulation for redundant functions between Wnt ligands during hair development, such as Wnt3a-deficiency (normally expressed in the IRS) where a hair phenotype has not been observed probably due to redundancy with Wnt10a in the IRS [44]. Thus, although in later stages of anagen progression (and hair differentiation) several different Wnt ligands including Wnt10b (Mx and IRS), Wnt4 (Mx), Wnt 10a (IRS), Wnt3a (IRS), Wnt3 (HS), Wnt11 (ORS) and Wnt5a (ORS, IRS) have been described previously [23], their abundant expression in several different HF compartments were not able to compensate fully for the loss of Wnt7b *in vivo* in our study.

Wnt7b is required to maintain normal anagen length and proper timing for catagen onset

By employing our K14-driven, Wnt7b loss-of-function model we revealed aberrant HF cycle progression in Wnt7b cKO mice. We confirmed efficient recombination events in Wnt7b cKO skin where Wnt7b had been effectively deleted and observed a striking postnatal hair phenotype in Wnt7b cKO mutant pups which presented delayed, restricted down growth and thinner hair coat production (Fig. 1F–J'). Furthermore, examination of the Wnt7b cKO HF cycle revealed a shorter anagen growth phase and premature catagen onset in transgenic mice (Fig. 2A, B), which resulted in overall HS length reduction approximately 30–40% (Fig. 2E, F). Indeed, we observed high Wnt7b expression in the hair bulb Mx progenitors during anagen (Fig. 2G, J, J'), which corresponds well to the localization of previously described canonical Wnt signaling components like strong nuclear β-cat stabilization and Lef-1 co-expression in the Mx area of the HF bulb [21, 40, 45, 46].

Interestingly, although entry to catagen was accelerated, we did not observe a change in the overall length of the catagen in Wnt7b-deficient HFs (Fig. 2B). These findings could imply that, due to loss of Wnt7b-mediated signaling, the resulting imbalance of Wnt signaling occurring subsequently during anagen, is responsible for precocious catagen onset and indirectly accelerates cell apoptosis and HF involution without changing the length of the catagen phase (Fig.7, Catagen).

Our data are in the agreement to recent publications that indicate the role of Wnt inhibition by DKK1 in promoting the transition from anagen towards catagen degeneration [47] and Wnt activators like Wnt10b which promote hair shaft growth and Mx proliferation [48–50]. Thus, our data reveal an additional Wnt ligand component, Wnt7b, to this model and demonstrate that shifting the balance between Wnt activators and Wnt inhibitors is an important means with which to drive hair towards growth or degeneration [47]. In addition, our findings are also consistent with previously described functions of Wnt7b (in different organ systems) in the stimulation of epithelium and mesenchyme replication in embryonic lung growth [30] and in proper placenta development [33]. Together, our findings suggest that Wnt7b acts in a non-redundant manner upon HF progenitors to support their proliferation and determine overall

anagen length and HS production (Fig. 2–4) while indirectly affecting catagen entry (without changing the length) by balancing Wnt activators – inhibitors ratio.

Wnt7b loss affects proper hair follicle development

Our analysis revealed diminished HF differentiation marker expression in Wnt7b cKO mutants and suggested a potential role for Wnt7b in normal HF differentiation events. Significantly, Wnt7b-null hair displayed proper hair structure and, although all hair types were produced, Wnt7b cKO HFs were considerably thinner and smaller in size than Con HFs. Previously, canonical Wnt signaling with nuclear β-cat stabilization and Lef-1 co-expression has been observed in Mx cells of growing hair [21, 46] and Lef1-deficient mice developed few incompletely keratinized hairs [40]. These data directly correlate with activity of a Wnt-responsive B-galactosidase reporter gene in TOPGAL or BAT-gal mice, where pre-cortical and cortical layers of matrix progenitor cells of future hair shafts were positively marked [20, 21]. Indeed, in our results we observed reduced nuclear expression of Lef-1, a co-transcription factor of the canonical Wnt pathway directly interacting with β-catenin, and less Mx progenitor cells expressing nuclear Lef1 and β-catenin in growing Wnt7b cKO HFs. However further analysis of Wnt7b in different HFs layer specification is needed to fully explain the observed differentiation defect.

Wnt7b is important to activate and promote normal telogen to anagen transition in hfSCs

During the normal telogen-anagen transition, the balance between activators and inhibitors within the hair bulge where hfSCs reside may influence whether a HF is primed to re-enter anagen [28]. We have previously reported that BMP signaling is critical for maintaining hfSCs quiescence during telogen [32] and upon BMP inhibition, hfSCs tilt towards activation [28]. Recently we revealed that Wnt7b is a putative BMP target gene in hfSCs and is up-regulated in the hair germ and hfSCs population following BMP inhibition during the physiological telogen-anagen transition [28] (Fig.7, telogen-anagen). Here, we demonstrated that targeted, postnatal ablation of Wnt7b in hfSCs resulted in delayed telogen-anagen transition *in vivo*, thereby supporting our previous findings and suggesting that Wnt7b is an important additional component involved in driving hfSCs activation, possibly acting with other Wnt ligands (Fig.7, telogen-anagen). Previously we described the function of another BMP signaling target gene, WNT7a, as an intrinsic activator of quiescent hfSCs *in vivo* via a canonical Wnt mechanism and here we validate another intrinsic Wnt ligand, Wnt7b as a direct target of canonical BMP signaling in hfSCs (Fig, 6B). Although we have not detected up-regulation of other Wnt ligands except of Wnt16 during early telogen to anagen transition upon BMP inhibition in hfSCs [28], our data suggest that both Wnt7a and Wnt7b may co-operate to activate the canonical Wnt pathway at the onset of anagen entry. Interestingly, hfSCs lacking Wnt7b were able to proceed into new anagen growth suggesting partial Wnt compensation. However, full anagen down growth could not be reached following Wnt7b deficiency demonstrating that loss of Wnt7b cannot be fully compensated *in vivo*. In addition, we also confirmed that the delay in postnatal T-A transition in Wnt7b cKO HF was caused by postponed cells activation, primarily in HG and secondary in bulge, and although delayed, cells still demonstrated similar sequence of stimulation as previously observed in normal HFs [10]. We also showed that the delay in T-A transition in Wnt7b cKO HF was not a direct consequence in overall differences of the stem cell numbers forming the

first postnatal telogen bulge, since the amount of hfSCs in both Con and Wnt7b cKO was similar and not affected. Furthermore, although in Wnt7b-deficient HFs we observed unaffected stem cell numbers in the telogen bulges and Wnt7b cKO hfSCs were still capable of participating in and reforming the new HF bulges during following hair cycles, however the enrichment of Wnt7b cKO hfSCs in this process was significantly slower when compared to Con, suggesting that right tuning of WNT signaling is important in proper self-renewal of hfSCs. Thus, our results support an intrinsic and non-redundant function of Wnt7b in promoting HG and bulge hfSCs activation, without affecting hfSCs number during bulge formation. However, Wnt7b-deficiency does disturb the overall hfSCs self-renewal dynamic primarily affecting their efficiency to re-populate HF bulge.

Comparative analysis of mouse Wnt7a and Wnt7b protein sequences (Fig. S6A–B) revealed approximately 76% homology. Although to date, little is known about the precise mechanisms of the ligand-Fzd receptor interactions of Wnt7a and Wnt7b *in vivo*, there is published *in vitro* data, suggesting that Wnt7a may have differing affinity with certain Fzd receptors [51]. Interestingly, our previously published work [28], indicates that during hfSCs activation at T-A transition after BMP inhibition, one potential candidate receptor for both Wnt7a and Wnt7b may be Fzd10 as this was the only up-regulated Fzd receptor observed in our array data and we demonstrated its protein expression within the HG of activated HFs. Recently, Wnt10b over-expression was reported to induce HF activation via a canonical Wnt mechanism [50]. Thus, it is interesting to speculate that after hfSCs activation, the HG and transit amplifying (TA) progenitors of the ORS and Mx can sum up the total Wnt ligands to reach an optimal canonical Wnt activation level required for proper hair proliferation and growth (Fig.7, Full anagen). It also suggests that although expression of different Wnt ligands could be redundant during the anagen phase of the hair cycle, surprisingly loss of one Wnt ligand from the intrinsic compartment (either hfSCs, HG or ORS or Mx) cannot be fully substituted by others (either intrinsic or extrinsic Wnt ligands), indicating that the level of β-catenin is very tightly regulated to prevent uncontrolled overgrow or even tumor initiation. Indeed, a recently published study reported that during basal cell carcinoma (BCC) initiation following oncogenic SmoM2 expression, Wnt7b expression was elevated and promoted the reprogramming of adult interfollicular cells into embryonic HF progenitors, also suggesting that β-catenin regulates an amplification loop that sustains both Wnt and Hedgehog signaling which interact together to initiate BCC formation [52]. These results are also interesting in the light of a recently published report describing that Wnt7b mediates autocrine (intrinsic) canonical Wnt dependent signaling in anchorage-independent growth in pancreatic adenocarcinoma [53].

Finally, our findings are also in agreement with the view that the resting, telogen phase of the hair cycle is divided into two phases, a competent telogen where HFs cannot re-enter anagen and a refractory telogen in which HFs become increasingly primed for activation [54, 55](Fig. 7, Telogen). We observed a significant delay in hfSCs activation following Wnt7b ablation, suggesting Wnt7b may be a critical signaling mediator (possibly working in conjunction with Wnt7a [28]), which is up-regulated during refractory telogen upon BMP inhibition, thereby priming and tilting the balance towards HF activation.

In summary, we have revealed a non-redundant function for Wnt7b in HF cycle length determination and a partially redundant role in hfSCs activation during physiological telogen-anagen transition. These findings have potential applications in the development of therapies for HF–related diseases and future studies could unravel the precise underlying mechanisms of Wnt7b-regulated hfSCs and TA-progenitors activation, exploring its therapeutic potential.

Supplementary Material

Refer to Web version on PubMed Central for supplementary material.

ACKNOWLEDGEMENTS

We thank the USC Animal Facility for mouse husbandry. This study was supported initially by the Donald E. and Delia B. Baxter Foundation Award for K.K and National Institute of Arthritis and Musculoskeletal and Skin Diseases of the National Institutes of Health Grants R01-AR061552 (to K.K.), and R03-AR061028 (to K.K.), E.K is a fellow of the California Institute for Regenerative Medicine (CIRM) – Research Training Program II in Stem Cell Biology.

REFERENCES

1. Hardy MH. The secret life of the hair follicle. Trends Genet. 1992; 8:55–61. [PubMed: 1566372]
2. Millar SE. Molecular mechanisms regulating hair follicle development. J Invest Dermatol. 2002; 118:216–225. [PubMed: 11841536]
3. Sengel P, Mauger A. Peridermal cell patterning in the feather-forming skin of the chick embryo. Dev Biol. 1976; 51:166–171. [PubMed: 950073]
4. Muller-Rover S, Peters EJ, Botchkarev VA, et al. Distinct patterns of NCAM expression are associated with defined stages of murine hair follicle morphogenesis and regression. J Histochem Cytochem. 1998; 46:1401–1410. [PubMed: 9815282]
5. Blanpain C, Lowry WE, Geoghegan A, et al. Self-renewal, multipotency, and the existence of two cell populations within an epithelial stem cell niche. Cell. 2004; 118:635–648. [PubMed: 15339667]
6. Cotsarelis G, Sun TT, Lavker RM. Label-retaining cells reside in the bulge area of pilosebaceous unit: implications for follicular stem cells, hair cycle, and skin carcinogenesis. Cell. 1990; 61:1329–1337. [PubMed: 2364430]
7. Fuchs E, Tumbar T, Guasch G. Socializing with the neighbors: stem cells and their niche. Cell. 2004; 116:769–778. [PubMed: 15035980]
8. Trempus CS, Morris RJ, Bortner CD, et al. Enrichment for living murine keratinocytes from the hair follicle bulge with the cell surface marker CD34. J Invest Dermatol. 2003; 120:501–511. [PubMed: 12648211]
9. Morris RJ, Liu Y, Marles L, et al. Capturing and profiling adult hair follicle stem cells. Nat Biotechnol. 2004; 22:411–417. [PubMed: 15024388]
10. Greco V, Chen T, Rendl M, et al. A two-step mechanism for stem cell activation during hair regeneration. Cell Stem Cell. 2009; 4:155–169. [PubMed: 19200804]
11. Panteleyev AA, Jahoda CA, Christiano AM. Hair follicle predetermination. J Cell Sci. 2001; 114:3419–3431. [PubMed: 11682602]
12. Niemann C, Owens DM, Hulsken J, et al. Expression of DeltaNLef1 in mouse epidermis results in differentiation of hair follicles into squamous epidermal cysts and formation of skin tumours. Development. 2002; 129:95–109. [PubMed: 11782404]
13. Lee J, Tumbar T. Hairy tale of signaling in hair follicle development and cycling. Semin Cell Dev Biol. 2012; 23:906–916. [PubMed: 22939761]
14. Fuchs E, Merrill BJ, Jamora C, et al. At the roots of a never-ending cycle. Dev Cell. 2001; 1:13–25. [PubMed: 11703920]

15. Alonso LC, Rosenfield RL. Molecular genetic and endocrine mechanisms of hair growth. Horm Res. 2003; 60:1–13. [PubMed: 12792148]
16. Lei M, Yang T, Lai X, et al. Upregulation of interfollicular epidermal and hair infundibulum beta-catenin expression in Gsdma3 mutant mice. Acta Histochem. 2013; 115:63–69. [PubMed: 22694914]
17. Millar SE, Willert K, Salinas PC, et al. WNT signaling in the control of hair growth and structure. Dev Biol. 1999; 207:133–149. [PubMed: 10049570]
18. Huelsken J, Vogel R, Erdmann B, et al. beta-Catenin controls hair follicle morphogenesis and stem cell differentiation in the skin. Cell. 2001; 105:533–545. [PubMed: 11371349]
19. Gat U, DasGupta R, Degenstein L, et al. De Novo hair follicle morphogenesis and hair tumors in mice expressing a truncated beta-catenin in skin. Cell. 1998; 95:605–614. [PubMed: 9845363]
20. Maretto S, Cordenonsi M, Dupont S, et al. Mapping Wnt/beta-catenin signaling during mouse development and in colorectal tumors. Proc Natl Acad Sci U S A. 2003; 100:3299–3304. [PubMed: 12626757]
21. DasGupta R, Fuchs E. Multiple roles for activated LEF/TCF transcription complexes during hair follicle development and differentiation. Development. 1999; 126:4557–4568. [PubMed: 10498690]
22. Reddy ST, Andl T, Lu MM, et al. Expression of Frizzled genes in developing and postnatal hair follicles. J Invest Dermatol. 2004; 123:275–282. [PubMed: 15245425]
23. Reddy S, Andl T, Bagasra A, et al. Characterization of Wnt gene expression in developing and postnatal hair follicles and identification of Wnt5a as a target of Sonic hedgehog in hair follicle morphogenesis. Mech Dev. 2001; 107:69–82. [PubMed: 11520664]
24. Andl T, Reddy ST, Gaddapara T, et al. WNT signals are required for the initiation of hair follicle development. Dev Cell. 2002; 2:643–653. [PubMed: 12015971]
25. Widelitz RB, Jiang TX, Lu J, et al. beta-catenin in epithelial morphogenesis: conversion of part of avian foot scales into feather buds with a mutated beta-catenin. Dev Biol. 2000; 219:98–114. [PubMed: 10677258]
26. Lowry WE, Blanpain C, Nowak JA, et al. Defining the impact of beta-catenin/Tcf transactivation on epithelial stem cells. Genes Dev. 2005; 19:1596–1611. [PubMed: 15961525]
27. Lo Celso C, Prowse DM, Watt FM. Transient activation of beta-catenin signalling in adult mouse epidermis is sufficient to induce new hair follicles but continuous activation is required to maintain hair follicle tumours. Development. 2004; 131:1787–1799. [PubMed: 15084463]
28. Kandyba E, Leung Y, Chen YB, et al. Competitive balance of intrabulge BMP/Wnt signaling reveals a robust gene network ruling stem cell homeostasis and cyclic activation. Proc Natl Acad Sci U S A. 2013; 110:1351–1356. [PubMed: 23292934]
29. Vasioukhin V, Degenstein L, Wise B, et al. The magical touch: genome targeting in epidermal stem cells induced by tamoxifen application to mouse skin. Proc Natl Acad Sci U S A. 1999; 96:8551–8556. [PubMed: 10411913]
30. Rajagopal J, Carroll TJ, Guseh JS, et al. Wnt7b stimulates embryonic lung growth by coordinately increasing the replication of epithelium and mesenchyme. Development. 2008; 135:1625–1634. [PubMed: 18367557]
31. Srinivas S, Watanabe T, Lin CS, et al. Cre reporter strains produced by targeted insertion of EYFP and ECFP into the ROSA26 locus. BMC Dev Biol. 2001; 1:4. [PubMed: 11299042]
32. Kobielak K, Stokes N, de la Cruz J, et al. Loss of a quiescent niche but not follicle stem cells in the absence of bone morphogenetic protein signaling. Proc Natl Acad Sci U S A. 2007; 104:10063–10068. [PubMed: 17553962]
33. Parr BA, Cornish VA, Cybulsky MI, et al. Wnt7b regulates placental development in mice. Dev Biol. 2001; 237:324–332. [PubMed: 11543617]
34. Kobielak K, Pasolli HA, Alonso L, et al. Defining BMP functions in the hair follicle by conditional ablation of BMP receptor IA. J Cell Biol. 2003; 163:609–623. [PubMed: 14610062]
35. Kandyba E, Hazen VM, Kobielak A, et al. Smad1&5 but not Smad8 establish stem cell quiescence which is critical to transform the premature hair follicle during morphogenesis towards the Postnatal State. Stem Cells. 2013

36. Beaudoin GM 3rd, Sisk JM, Coulombe PA, et al. Hairless triggers reactivation of hair growth by promoting Wnt signaling. Proc Natl Acad Sci U S A. 2005; 102:14653–14658. [PubMed: 16195376]
37. Huelsken J, Behrens J. The Wnt signalling pathway. J Cell Sci. 2002; 115:3977–3978. [PubMed: 12356903]
38. Ito M, Yang Z, Andl T, et al. Wnt-dependent de novo hair follicle regeneration in adult mouse skin after wounding. Nature. 2007; 447:316–320. [PubMed: 17507982]
39. Schlake T, Sick S. Canonical WNT signalling controls hair follicle spacing. Cell Adh Migr. 2007; 1:149–151. [PubMed: 19262137]
40. Kratochwil K, Dull M, Farinas I, et al. Lef1 expression is activated by BMP-4 and regulates inductive tissue interactions in tooth and hair development. Genes Dev. 1996; 10:1382–1394. [PubMed: 8647435]
41. van Genderen C, Okamura RM, Farinas I, et al. Development of several organs that require inductive epithelial-mesenchymal interactions is impaired in LEF-1-deficient mice. Genes Dev. 1994; 8:2691–2703. [PubMed: 7958926]
42. Nguyen H, Merrill BJ, Polak L, et al. Tcf3 and Tcf4 are essential for long-term homeostasis of skin epithelia. Nat Genet. 2009; 41:1068–1075. [PubMed: 19718027]
43. Chan EF, Gat U, McNiff JM, et al. A common human skin tumour is caused by activating mutations in beta-catenin. Nat Genet. 1999; 21:410–413. [PubMed: 10192393]
44. Greco TL, Takada S, Newhouse MM, et al. Analysis of the vestigial tail mutation demonstrates that Wnt-3a gene dosage regulates mouse axial development. Genes Dev. 1996; 10:313–324. [PubMed: 8595882]
45. Zhou P, Byrne C, Jacobs J, et al. Lymphoid enhancer factor 1 directs hair follicle patterning and epithelial cell fate. Genes Dev. 1995; 9:700–713. [PubMed: 7537238]
46. Merrill BJ, Gat U, DasGupta R, et al. Tcf3 and Lef1 regulate lineage differentiation of multipotent stem cells in skin. Genes Dev. 2001; 15:1688–1705. [PubMed: 11445543]
47. Kwack MH, Kim MK, Kim JC, et al. Dickkopf 1 promotes regression of hair follicles. J Invest Dermatol. 2012; 132:1554–1560. [PubMed: 22358062]
48. Ouji Y, Yoshikawa M, Moriya K, et al. Effects of Wnt-10b on hair shaft growth in hair follicle cultures. Biochem Biophys Res Commun. 2007; 359:516–522. [PubMed: 17548054]
49. Li YH, Zhang K, Ye JX, et al. Wnt10b promotes growth of hair follicles via a canonical Wnt signalling pathway. Clin Exp Dermatol. 2011; 36:534–540. [PubMed: 21392083]
50. Li YH, Zhang K, Yang K, et al. Adenovirus-mediated Wnt10b overexpression induces hair follicle regeneration. J Invest Dermatol. 2013; 133:42–48. [PubMed: 22832493]
51. Carmon KS, Loose DS. Development of a bioassay for detection of Wnt-binding affinities for individual frizzled receptors. Anal Biochem. 2010; 401:288–294. [PubMed: 20227380]
52. Youssef KK, Lapouge G, Bouvree K, et al. Adult interfollicular tumour-initiating cells are reprogrammed into an embryonic hair follicle progenitor-like fate during basal cell carcinoma initiation. Nat Cell Biol. 2012; 14:1282–1294. [PubMed: 23178882]
53. Arensman MD, Kovochich AN, Kulikauskas RM, et al. WNT7B mediates autocrine Wnt/beta-catenin signaling and anchorage-independent growth in pancreatic adenocarcinoma. Oncogene. 2013
54. Plikus MV, Mayer JA, de la Cruz D, et al. Cyclic dermal BMP signalling regulates stem cell activation during hair regeneration. Nature. 2008; 451:340–344. [PubMed: 18202659]
55. Plikus MV, Baker RE, Chen CC, et al. Self-organizing and stochastic behaviors during the regeneration of hair stem cells. Science. 2011; 332:586–589. [PubMed: 21527712]

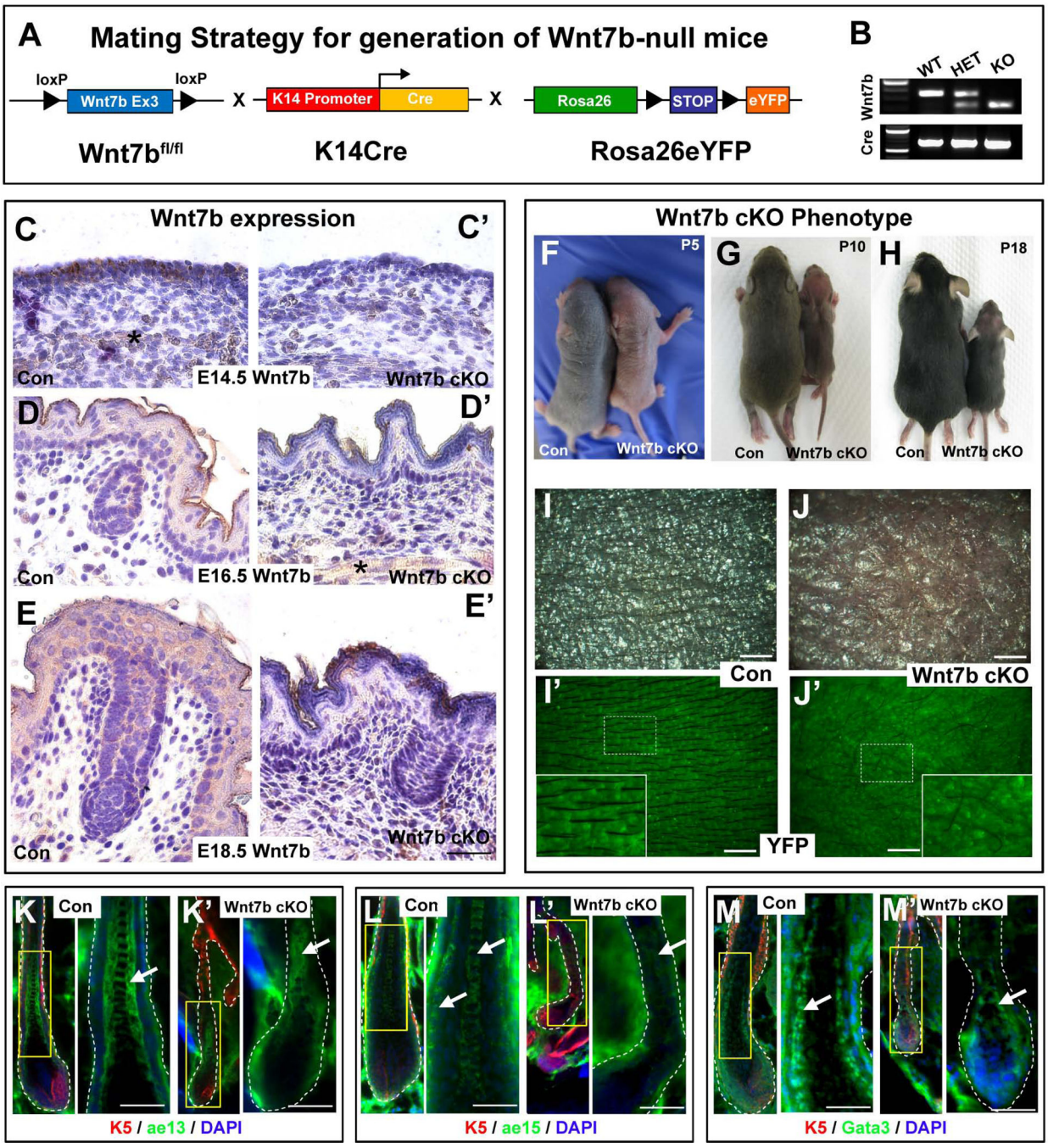

Figure 1. Generation of Wnt7b-null (Wnt7b cKO) transgenic mice with aberrant hair coat production and diminished hair differentiation marker expression

(A) Schematic representation of the mating strategy used to generate Wnt7b-deficient transgenic mice. Wnt7b$^{fl/fl}$ transgenic mice were crossed with K14Cre mice and Rosa26-STOP-eYFP reporter mice to generate offspring with Cre-mediated deletion of Wnt7b in K14+ YFP-labeled epithelial tissue. (B) PCR genotyping was used to distinguish YFP+ control (Con) and YFP+ Wnt7b-deficient mice (Wnt7b cKO). (C, D, E) Immunohistochemistry (IHC) directed against endogenous Wnt7b protein was performed on Con and (C', D', E') Wnt7b cKO dorsal back skin at E14.5, E16.5 and E18.5 to demonstrate

efficient deletion of Wnt7b in Wnt7b cKO transgenic mouse skin. All IHC images were counterstained with hematoxylin (blue) to label nuceli. (F–H) Phenotype of Con and Wnt7b cKO transgenic mice at postnatal day (P) P5 (F), P10 (G) and P18 (H). (I, I') Dorsal skin of P7 YFP+ Con mice displayed organized, visible hair shafts (HS) protruding from the skin surface. (J, J') Dorsal skin of P7 YFP+ Wnt7b cKO transgenic mice displayed disorganized, aberrant and fewer hair shafts at the skin surface. Immunofluorescence directed against known hair follicle differentiation markers K5 (red, K–M'), ae13 (green, K, K'), ae15 (green; L, L') and Gata3 (green, M, M') in Con (K, L, M) and Wnt7b cKO transgenic (K', L', M') hair follicles. DAPI (blue) counterstaining was used to label cell nuclei (K–M'). Asterisk labels subcutaneous muscle stained positive (brown) for Wnt7b. Scale bar = 50μm.

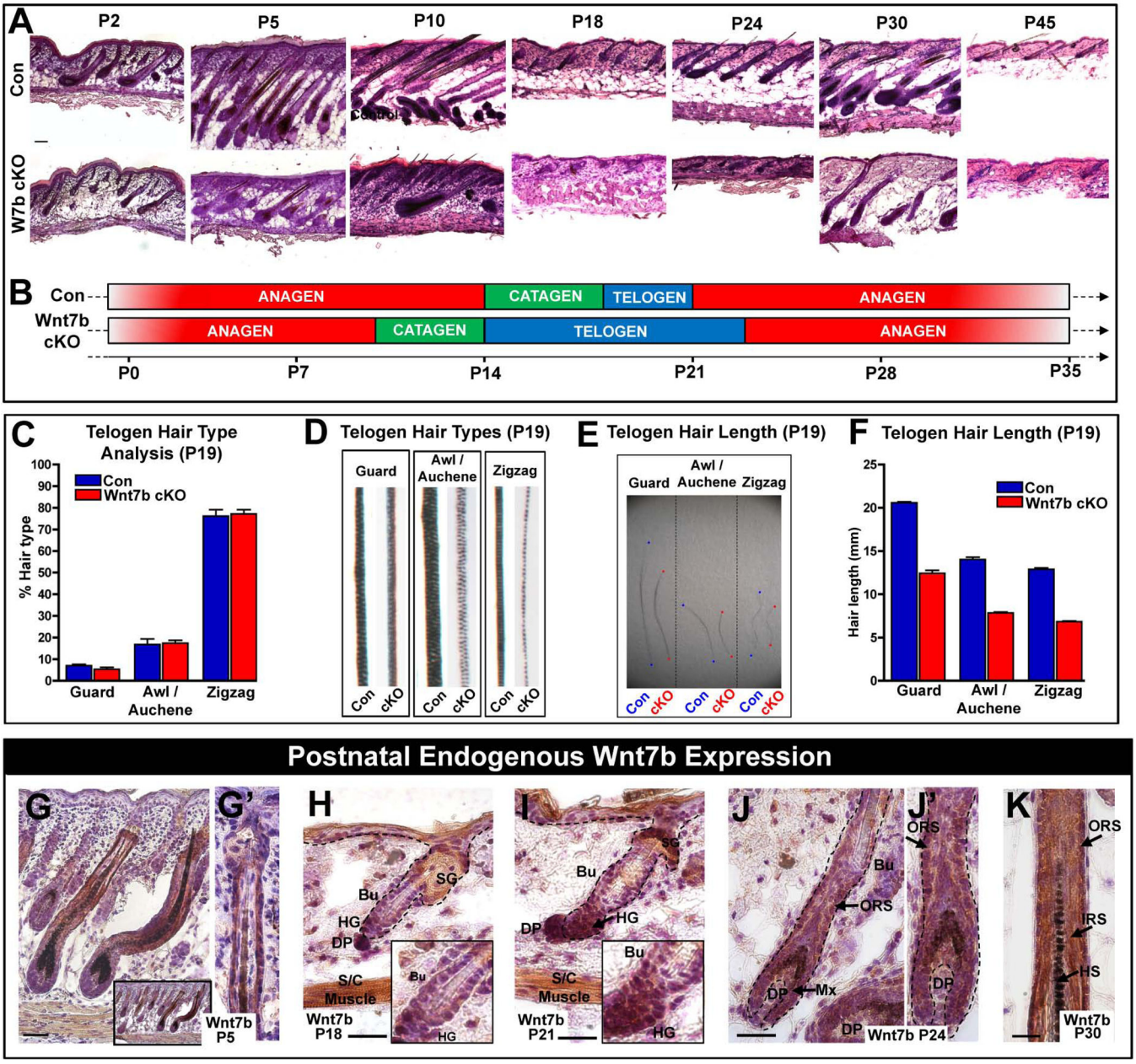

Figure 2. Wnt7b-deficient transgenic mice display aberrant hair follicle cycling

(A) Postnatal hair follicle (HF) cycle in Con and Wnt7b cKO transgenic mice (P5–45). (B) Schematic illustrating perturbed HF cycle in Wnt7b cKO mice compared with Con littermates. (C–F) Analysis of plucked, telogen (P19) hairs from Con and Wnt7b cKO mice. (C) Comparison of different HF types of Wnt7b cKO and Con mice. (D) Comparison of the hair shaft structure of Wnt7b cKO and Con mice. (E, F) Length of different hair types from Wnt7b cKO and Con HFs. (G, G') Wnt7b expression in the ORS cells of P5 anagen HFs. (H, I and insets) Changes in Wnt7b expression during telogen to anagen transition between P18 and P21, strong cytoplasmic Wnt7b expression in the enlarged, activated HG and lower hfSCs (Bu) at anagen onset P21 compared to P18. (J, J' magnification) At P24, during the first postnatal anagen, Wnt7b is expressed in the ORS, matrix progenitor cells and in the

differentiating layers at P30 (K). All IHC images were counterstained with hematoxylin (blue) to label nuceli. Insets depict magnified regions within the figure. Abbreviations: P, postnatal day; DP, dermal papillae; SG, sebaceous gland; ORS, outer root sheath; HS, hair shaft; HFs; hair follicle; Bu, bulge; HG, hair germ; hfSCs, hair follicle stem cells; S/C. subcutaneous; IRS, inner root sheath. Scale bar = 50μm.

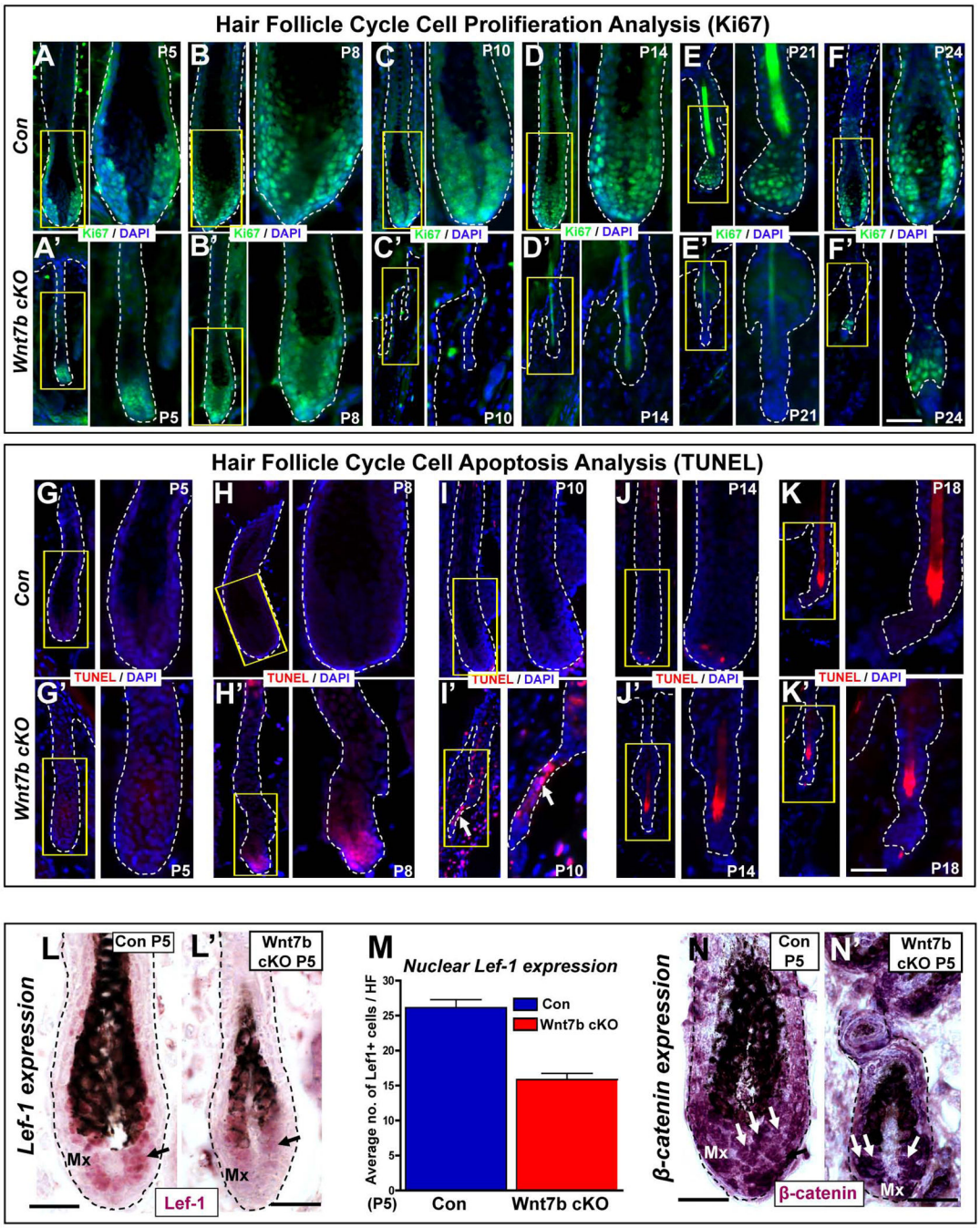

Figure 3. Wnt7b ablation results in a shorter hair cycle with premature catagen onset and delayed anagen entry

(A–F') Immunofluorescence targeting the cell proliferation marker, Ki67 (green) during the postnatal hair cycle (from P5–P24) in Con (A–F) and Wnt7b cKO (A'–F') mice. TUNEL staining (red) was used to detect cell apoptosis and indicate initiation of the degenerative hair follicle phase, catagen, in Con (G–K) and Wnt7b cKO (G'–K') hair follicles. DAPI (blue) counterstaining was used to label cell nuclei. Arrow marks the TUNEL positive, degenerating epithelial strand. Immunohistochemistry (IHC) detecting nuclear Lef-1 (purple) in Con (L) and Wnt7b cKO (L') at P5 with quantification of the number of nuclear

Lef-1 positive cells per HF (M). (N–N') IHC targeting β-catenin expression in P5 Con (N) and Wnt7b cKO (N') HFs. Scale bar = 50μm.

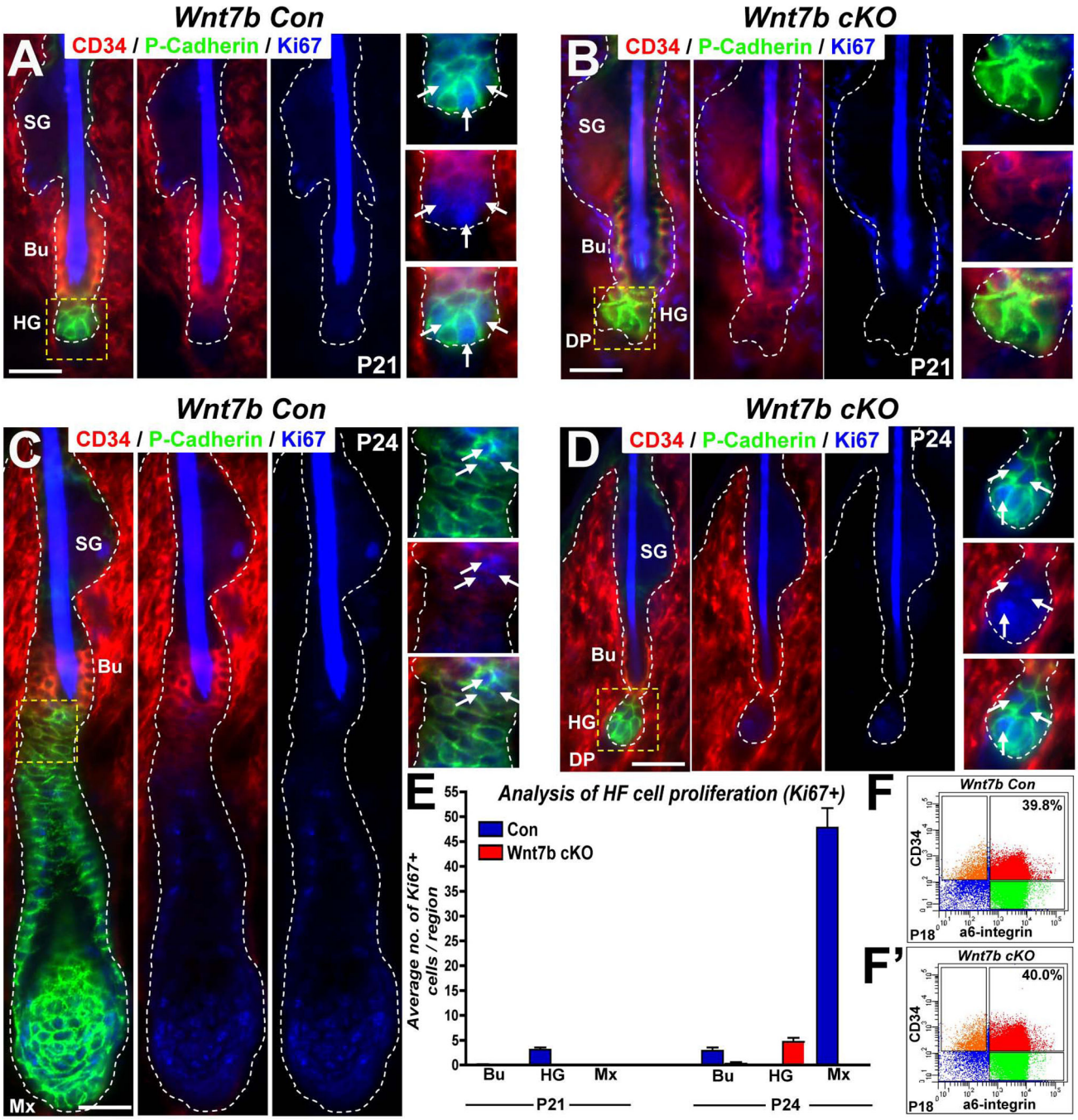

Figure 4. Wnt7b-deficiency does not perturb the sequential "two-step" mechanism of HF activation during telogen-anagen transision

(A–D) Triple immunofluorescence (IF) targeting cell proliferation (Ki67, blue) in the bulge (Bu) hfSCs using CD34 (red) marker expression and the hair germ (HG) using P-cadherin (green) staining in Con (A, C) and Wnt7b cKO (B, D) HFs at P21 (A–B) and P24 (C–D). (E) Quantification of nuclear Ki67 IF in specific HF compartments (Bu, bulge hfSCs, HG, hair germ; Mx, matrix cells) at P21 and P24. (F–F') FACS analysis of P18 Con (F) and Wnt7b cKO (F') HFs employing CD34 and α6-integrin marker expression. α6-integrin^{High}/

CD34^{High} (red) denotes comparable total basal hfSCs (b-hfSCs) numbers in the bulge of Con (E, 39.8%) and Wnt7b cKO (E', 40%) HFs.

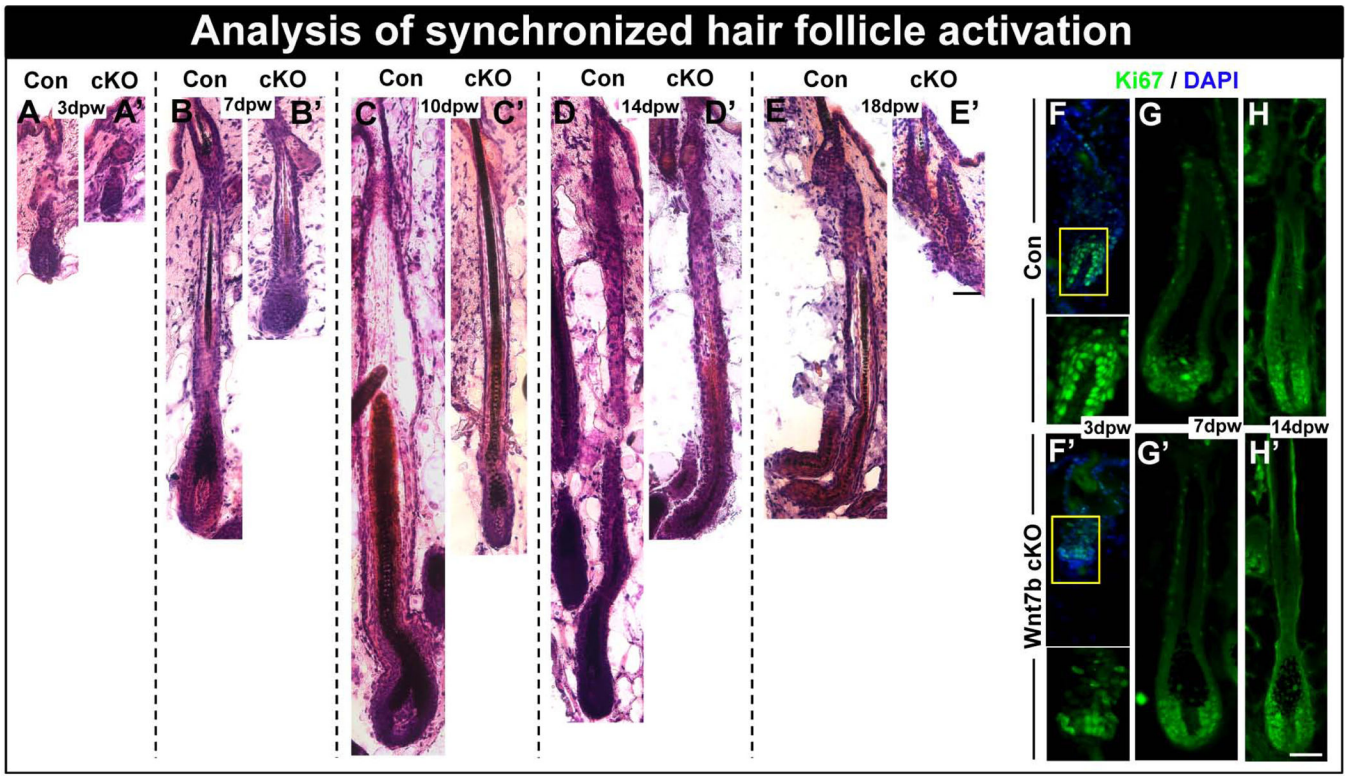

Figure 5. Wnt7b-deficient hair follicles display delayed anagen entry after hair cycle synchronization by depilation

(A–E') Con and Wnt7b cKO dorsal hair was waxed to synchronize hair follicle activation (promoting anagen entry) and hair re-growth monitored and stained by H&E. (A) After 3 days postwaxing (pw) Con HFs revealed HF downgrowth in early anagen with HFs extending into the subcutaneous fat layer, however, at the same time point (A'), Wnt7b cKO HF regrowth appeared delayed and remained more superficial to the epidermis. (B) At 7 days pw, Con anagen HFs extended deep into the subcutaneous fat tissue (B') whereas, Wnt7b cKO still remained delayed by comparison. (C) After 10 days pw, Con full anagen HFs produced thick, pigmented hair shafts, (C') however, Wnt7b cKO HFs appeared considerably thinner with delayed downgrowth into the dermis. (D) 14 days pw, Con HFs remained in anagen (D'), however, Wnt7b cKO HFs were in early catagen. (E) At 18 days pw, the lower portion of Con HFs were beginning to degenerate in catagen, whereas, Wnt7b cKO HFs had already transitioned to telogen (E'). (F–H') Immunofluorescence detecting Ki67 (green) in regenerating Con (F–H) and Wnt7b cKO (F'–H') HFs at 3dpw (F, F'), 7dpw (G, G') and 14dpw (H, H'). DAPI (blue) counterstaining was used to label cell nuclei in immunofluorescence images. Scale bar = 50μm.

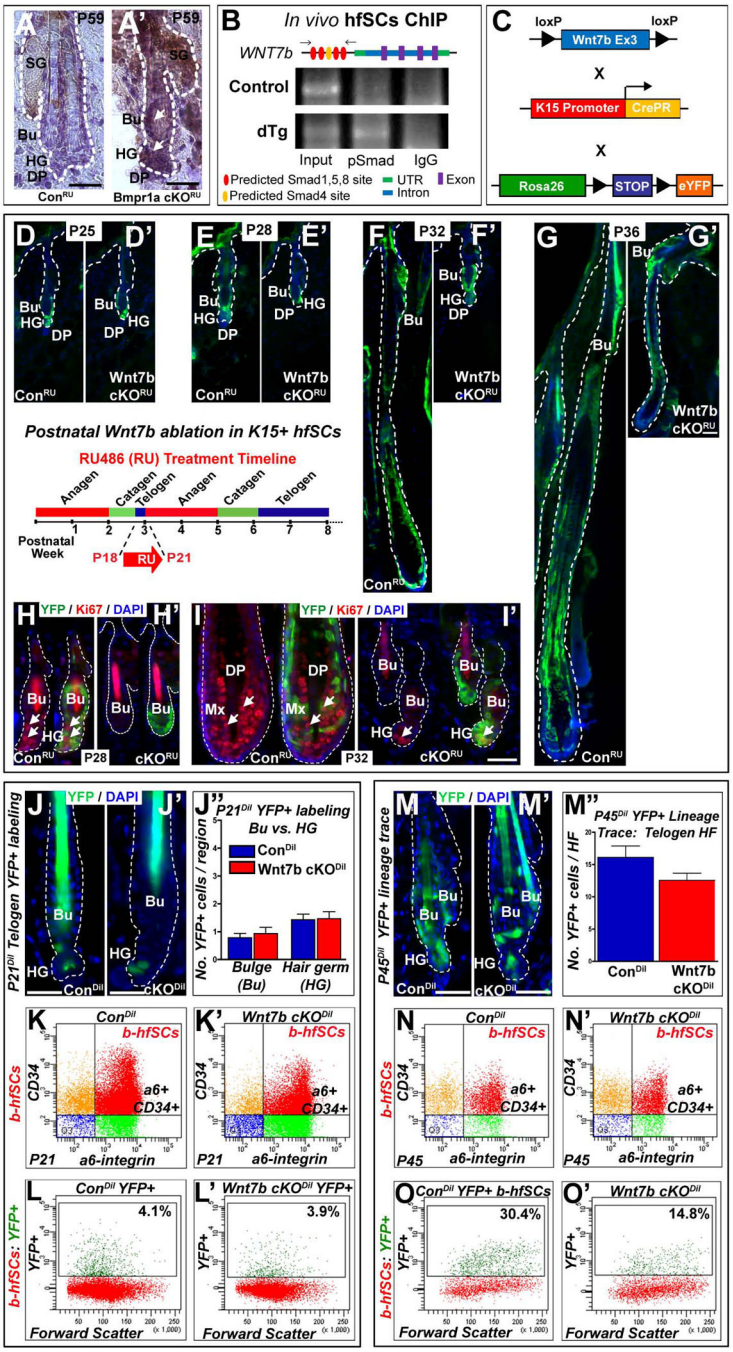

Figure 6. Delayed hair follicle stem cell (hfSCs) activation following Wnt7b ablation

(A') Up-regulation of WNT7b in telogen bulge (Bu) hfSCs and hair germ (HG) after BMP pathway inactivation in BMPR1A cKO^{RU} at P59 compared to Con^{RU} HFs (A) where WNT7b staining was absent. (B) *In vivo* hfSCs ChIP PCR reveals selective precipitation of DNA fragments that possess canonical Smad binding elements of Wnt7b promoter, flanking primers (arrows) in schematic (C) Schematic of transgenic mice generation with targeted Wnt7b deletion in the bulge: Con and Wnt7b$^{fl/fl}$ transgenic mice (both K15CrePR+; YFP+) were treated with RU486 from P18–P21 (schematic inset) to YFP label K15+ control

(Con^{RU}) and ablate Wnt7b in Wnt7b cKO^{RU} hfSCs. (D–G') The following postnatal hair cycle was monitored. (D, D') After 4 days (P25), both Con^{RU} and Wnt7b cKO^{RU} HFs remained in telogen due to RU treatment [35]. (E) By P28, YFP+ Con^{RU} HFs displayed telogen-anagen transition with enlarged, activated HG, however, YFP+ Wnt7b cKO^{RU} HFs remained in telogen (E'). At P32, YFP+ Con^{RU} HFs were in full anagen with efficient YFP+ labeling throughout all HF layers (F), however, YFP+ Wnt7b cKO^{RU} displayed enlarged HGs indicating initial HF activation and early telogen-anagen transition (F'). By P36, Con^{RU} YFP+ HFs were in full anagen with HFs extending deep into the dermis (G), whereas, Wnt7b cKO^{RU} YFP+ HFs were in early anagen (G'). (H–I') Immunofluorescence for the cell proliferation marker, Ki67 in YFP+ Con^{RU} and Wnt7b cKO^{RU} HFs. (H) At P28, Con^{RU} YFP+ HFs display strong nuclear Ki67 staining in the HG and lower Bu cells indicating HF activation, (H') however, Wnt7b cKO^{RU} HFs lacked Ki67 staining. (I) At P32, nuclear Ki67 staining was detected in the matrix cells of YFP+ Con^{RU} HFs. (I') Wnt7b cKO^{RU} YFP+ HFs displayed nuclear Ki67 staining in the HG indicating early HF activation. DAPI (blue) counterstaining was used to label all nuclei. Representative images of P21 Con^{Dil} (J) and Wnt7b cKO^{Dil} (J') YFP+ labeled HFs and quantification of the number of YFP+ cells per Bu and HG compartment (J"). (K–K') FACS analysis employing α6-integrin and CD34 staining with α6-integrin^{High}/CD34^{High} basal hfSCs population (b-hfSCs, red) in Con^{Dil} and Wnt7b cKO^{Dil} at P21 HFs. FACS analysis of b-hfSCs (α6^{High}/CD34^{High}) gated population for YFP positive cells in Con (L) and Wnt7b cKO (L') at P21 HFs. Representative images of P45 Con^{Dil} (M) and Wnt7b cKO^{Dil} (M') YFP+ labeled HFs and quantification of the number of YFP+ cells per HF (M"). (N–N') FACS analysis of α6-integrin and CD34 positive b-hfSCs population (b-hfSCs, red; α6-integrin^{High}/CD34^{High}) in Con^{Dil} and Wnt7b cKO^{Dil} at P45 HFs. FACS analysis of b-hfSCs (α6^{High}/CD34^{High}) gated population for YFP positive cells in Con^{Dil} (O) and Wnt7b cKO^{Dil} (O') at P45 HFs. Scale bar = 50μm.

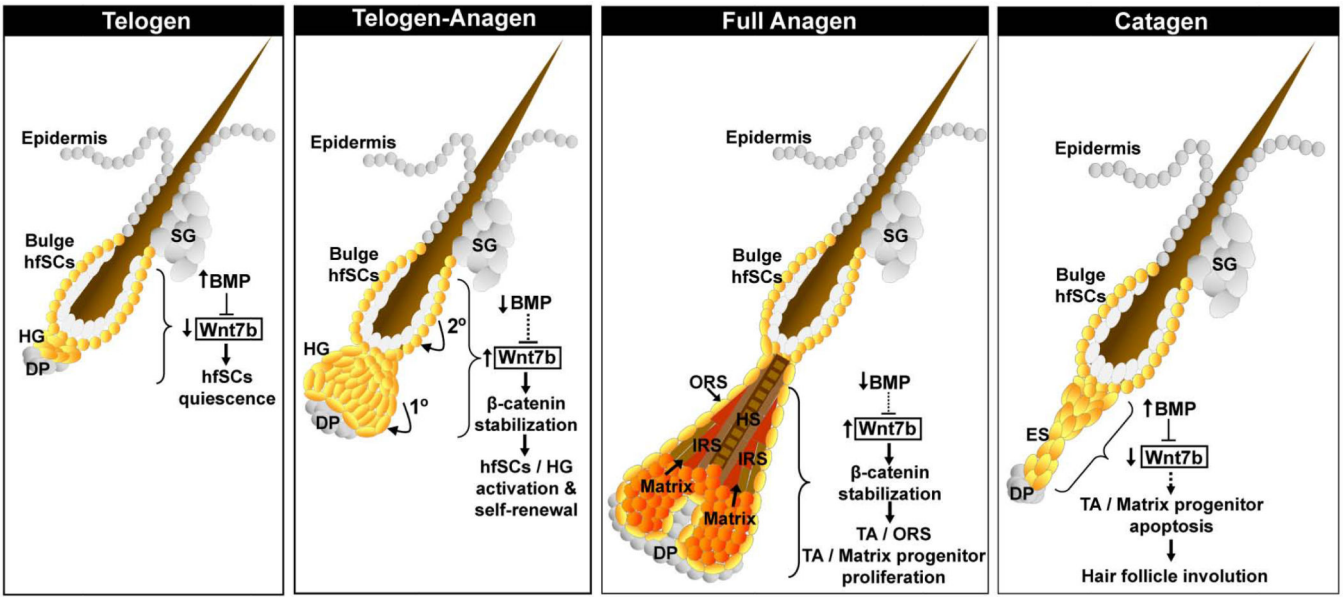

Figure 7. Model of the intrinsic role of Wnt7b and cross talk with BMP signaling in postnatal hair follicle stem cells (hfSCs) regulation and postnatal hair follicle cycling

Schematic model summarizing the role of Wnt7b in hfSCs during telogen and the telogen-anagen transition. During telogen-anagen transition, Wnt7b promotes a two-step sequence of HF stimulation, with initial activation in the HG (1°) and subsequently in the bulge hfSCs (2°). Proposed role for Wnt7b in matrix progenitor cells during the growth (anagen) and degenerative (catagen) phase of the postnatal hair follicle cycle. Loss of Wnt7b expression may indirectly be sufficient to promote HF involution by diminishing the collective WNT signaling during catagen (dotted arrow).